

1 **The push and pull of abandoned channels: How floodplain processes**
2 **and healing affect avulsion dynamics and alluvial landscape evolution**
3 **in foreland basins**

4 Harrison K. Martin¹, Douglas A. Edmonds¹

5 ¹Department of Earth and Atmospheric Sciences, Indiana University, Bloomington, Indiana, 47408, United States of America

6 *Correspondence to:* Harrison K. Martin (hkmartin@iu.edu)

7 **Abstract**

8 River avulsions are an important mechanism by which sediment is routed and emplaced in foreland basins. However, because
9 avulsions occur infrequently, we lack observational data that might inform where, when, and why avulsions occur and these
10 ~~questions-issues~~ are instead often investigated by rule-based numerical models. These models have historically simplified or
11 neglected the effects of abandoned channels on avulsion dynamics, even though fluvial megafans in foreland basins are
12 characteristically covered in abandoned channels. Here, we investigate the pervasiveness of abandoned channels on modern
13 fluvial megafan surfaces. Then, we present a physically based cellular model that parameterizes interactions between a single
14 avulsing river and abandoned channels in a foreland basin setting. We investigate how abandoned channels affect avulsion set-
15 up, pathfinding, and landscape evolution. We demonstrate and discuss how the processes of abandoned channel inheritance
16 and transient knickpoint propagation post-avulsion serve to shortcut the time necessary to set-up successive avulsions. Then,
17 we address the idea that abandoned channels can both repel and attract future pathfinding flows under different conditions. By
18 measuring the distance between the mountain-front and each avulsion over long (10^6 to 10^7 years) timescales, we show that
19 increasing abandoned channel repulsion serves to push avulsions farther from the mountain-front, while increasing attraction
20 pulls avulsions proximally. Abandoned channels do not persist forever, and we test possible channel healing scenarios
21 (deposition-only, erosion-only, and far-field directed) and show that only the final scenario achieves dynamic equilibrium
22 without completely filling accommodation space. We also observe megafan growth occurring via ~~10^4 -year~~~100,000 year
23 cycles of lobe switching, but only in our runs that employ deposition-only or erosion-only healing modes. Finally, we highlight
24 opportunities for future field work and remote sensing efforts to inform our understanding of the role that floodplain
25 topography, including abandoned channels, plays on avulsion dynamics.

Formatted: Font: Not Bold, Not Italic

Formatted: Font: Not Bold, Not Italic

Formatted: Font: Not Bold, Not Italic

1. Introduction

Avulsions, the wholesale relocations of rivers into new positions on their floodplains, are a primary control on how water and sediment are routed through alluvial landscapes (Mackey and Bridge, 1995). The predominant conceptual model presents avulsions as requiring two necessary components: a set-up, and a triggering event that causes bank failure and avulsion (Slingerland and Smith, 2004). However, there is a lack of observational data on each of these necessary components because avulsions occur infrequently (Edmonds et al., 2016). Instead, avulsion dynamics are often explored using concept-driven numerical models. One such form is cellular models, which seek to reduce the system to the components necessary to reproduce a natural phenomenon (Jerolmack and Paola, 2007). For planform avulsion models, this usually entails some description of sediment transport and deposition along an active channel and associated floodplain, and semi-heuristic rules for how avulsions are set-up, initiate, and pathfind (Hajek and Wolinsky, 2012). However, models have historically simplified or neglected the effect of abandoned channels on avulsion dynamics (Pelletier et al., 2005; Reitz et al., 2010). The relict topographic highs and lows associated with alluvial ridges, levees, and abandoned channels should affect both avulsion set-up and avulsion pathfinding ~~by repelling or attracting flows~~ (Leeder, 1977; Allen, 1978; Jerolmack and Paola, 2007; Reitz et al., 2010). ~~These effects could manifest as repulsion, if an approaching avulsing flow is restricted from entering an abandoned channel because of the unable to surmount topographic high created by the formed by remnant levees, or attraction, if flow is routed along the topographic lows of former channel pathways~~ (Edmonds et al., 2016).

The large, fan-shaped, low-relief fluvial megafans that exist where rivers leave lateral confinement and enter foreland basins are ideal locations to study the interaction between avulsions and abandoned channels (Fig. 1A; Leier et al., 2005; Weissmann et al., 2010). Fluvial megafans have some of the highest avulsion rates in the observational record (Valenza et al., 2020) and, in contrast to deltaic fans, have been qualitatively described as hosting abundant abandoned channels (e.g., Assine and Soares, 2004; Rossetti and Valeriano, 2007; Chakraborty et al., 2010; Bernal et al., 2011; Weissmann et al., 2013). However, we lack a detailed evaluation of the prevalence or distribution of this channelization, which is important to understand the degree to which avulsions may interact with abandoned channels.

In this paper, we present observational data on the channelization of fluvial megafan surfaces in alluvial foreland basin settings and we use these observations to motivate a physically based numerical model that parameterizes interactions between an avulsing river and abandoned channels in a subsiding basin. Our model implements tuneable abandoned channel dynamics that influence how abandoned channels affect pathfinding and are removed from the floodplain. Incorporating abandoned channel floodplain dynamics allows us to assess how abandoned channels affect where, when, and why avulsions occur. We demonstrate that abandoned channels, their interactions with future pathfinding flows, and the way they are removed from the floodplain are all important controls on avulsion locations, dynamics, and resulting foreland basin deposition and geomorphology that should be considered in future models and studies.

2. Background information

If abandoned channels are common features of megafan surfaces, they should also affect avulsion pathfinding on floodplain surfaces, it is reasonable to expect that they should affect how avulsions find new pathways. Despite this, most previous models have assumed abandoned channels have no effect on future avulsion pathfinding (Leeder, 1977; Ratliff et al., 2018), or act as universal repulsors (Allen, 1978; Bridge and Leeder, 1979) or universal attractors (Sun et al., 2002; Jerolmack and Paola, 2007; Reitz et al., 2010). The reality seems to be somewhere in-between these endmembers. ~~because. B b~~Both remote sensing (e.g. Edmonds et al., 2016; Valenza et al., 2020) and stratigraphic (e.g. Mohrig et al., 2000; Chamberlin and Hajek 2015, 2019) evidence suggests that avulsions commonly reoccupy former abandoned channel pathways. –However, if abandoned channels retain the superelevation that ~~once drove~~caused avulsion and abandonment, then that superelevation would topographically repel later pathfinding events (Leeder, 1977; Allen, 1978).

~~The earliest alluvial stratigraphy models that to connect avulsions to alluvial architecture encoded the effects of abandoned channels on avulsion pathfinding differently. were. H~~The pioneering Leeder (1977), Allen (1978), and Bridge and Leeder (1979) models. ~~These models connected avulsions to alluvial architecture by creating~~ 2D vertical slices of stratigraphy ~~that result~~resulting from channel avulsion across a basin over time. These models required heuristic rules about where successive rivers would be emplaced, including choosing locations randomly (Leeder, 1977), according to lowest elevation, (Bridge and Leeder, 1979), or randomly with additional elements of local abandoned channel repulsion (Allen, 1978). While their resulting stratigraphic sections were fairly insensitive to these differences (Hajek and Wolinsky, 2012), modern successors of these cross-section alluvial architecture models (e.g., Chamberlin and Hajek, 2015, 2019) have demonstrated that choosing different avulsion emplacement rules exerts a significant control on resulting stratigraphy. These rules position future channels along random (along a uniform distribution), compensational (at the lowest topographic elevation), or clustered (likelier to be nearer to the previous channel position) distributions. While these rules prescribe the cross-basin location of successive channels without needing to resolve planform pathfinding, and the compensation rule ~~intuitively reflects~~contains an essence of repulsion ~~by leaving behind~~as successive elevated abandoned alluvial ridges are left behind, it is unclear how flow routing due to abandoned channel repulsion or attraction further upstream affects or reflects each rule.

To avoid making explicit assumptions about channel emplacement, a parallel lineage of avulsion models resolve avulsion dynamics and pathfinding in a planform basin. ~~As such, t~~These avulsion models necessarily require rules for hydrodynamics, sediment transport, and avulsion set-up, initiation, pathfinding, and stabilization, but allow for a more sophisticated interaction between avulsion pathfinding and floodplain topography (including abandoned channels) than can be resolved in cross-section models (Hajek and Wolinsky, 2012). Whenever these models incorporate topographic steepness (with or without random noise) into avulsion pathfinding, and do not instantly erase the topographic alterations made by abandoned channels on landscapes, pathfinding is ~~implicitly~~controlled by abandoned channels (e.g., Mackey and Bridge, 1995; Coulthard et al., 2002; Sun et al., 2002; Jerolmack and Paola, 2007; Reitz et al., 2010).

90 In addition to affecting avulsion dynamics, the rate at which these abandoned channels (and associated alluvial ridges
91 and scours) are removed should affect ~~avulsion pathfinding and hence~~ landscape evolution. There are ~~very few~~not many
92 observations of abandoned channel healing rates, and those that exist are generally limited to sedimentation rates in oxbow
93 lakes hydraulically connected to active channels (e.g. Cooper and McHenry 1989; Rowland et al., 2005; Wren et al., 2008;
94 Kołaczek et al., 2017). As such, it is unclear in models whether to treat abandoned channels as healing instantly, persisting
95 indefinitely, or some intermediary. As a broad classification, there are at least four assumptions that can describe the fate of
96 these abandoned channels: i) avulsed channels do not leave behind abandoned channels on floodplains (instant healing; Ratliff
97 et al., 2018, 2021), ii) abandoned channels do not change after avulsion (no healing), iii) abandoned channels are instantly
98 healed after some fixed number of timesteps (Reitz et al., 2010), or iv) abandoned channels are healed gradually over time by
99 adjusting their channel-base and/or levee-top elevations (Jerolmack and Paola, 2007). The first three assumptions do not allow
100 abandoned channels to act as both repulsors and attractors, which is inconsistent with observations of avulsing rivers (Edmonds
101 et al., 2016; Valenza et al., 2020). Further, the first assumption generates no abandoned channel topography on floodplains
102 whatsoever.

103 Additionally, if one assumes that abandoned channels do heal, the mode of abandoned channel healing is unclear.
104 While little is known about the constructive and destructive processes in action on floodplains, we can speculate on the
105 evolution of abandoned channels using observations from both degradational and aggradational settings (Hartley et al., 2010b).
106 During floods, overbank sediments can preferentially deposit in abandoned channel topographic lows (Wolman and Eiler,
107 1958; Schmudde, 1963; Bridge and Leeder, 1979; Lewis and Lewin, 1983; Farrell, 1987; Nanson and Croke, 1992; Tooth et
108 al., 2002; Jerolmack and Paola, 2007; Toonen et al., 2012). This 'bottom-up' healing, however, can be undone in some cases
109 by scouring from future flooding events (Wolman and Leopold, 1957; Wolman and Eiler, 1958; Schmudde, 1963; Bridge and
110 Leeder, 1979). ~~the relative degree of levee erosion ('top-down' healing) is unknown. Top-down healing is plausible if a~~
111 ~~combination of diffusive sediment transport, weathering, and fluvial erosion during floods erode topographic highs on the~~
112 ~~floodplain (Hack and Goodlett, 1960; Burkham, 1972; Zwoliński, 1992; Gabet, 2000; Croke et al., 2013). In summary,~~
113 ~~however, there are unanswered questions about the fates and rates of abandoned channel floodplain topography. These~~
114 ~~questions have important implications for the gross morphology of foreland basins and their deposits because the primary~~
115 ~~mode of sediment transport and emplacement in this depositional environment is via alluvium deposited by and between~~
116 ~~avulsions.~~

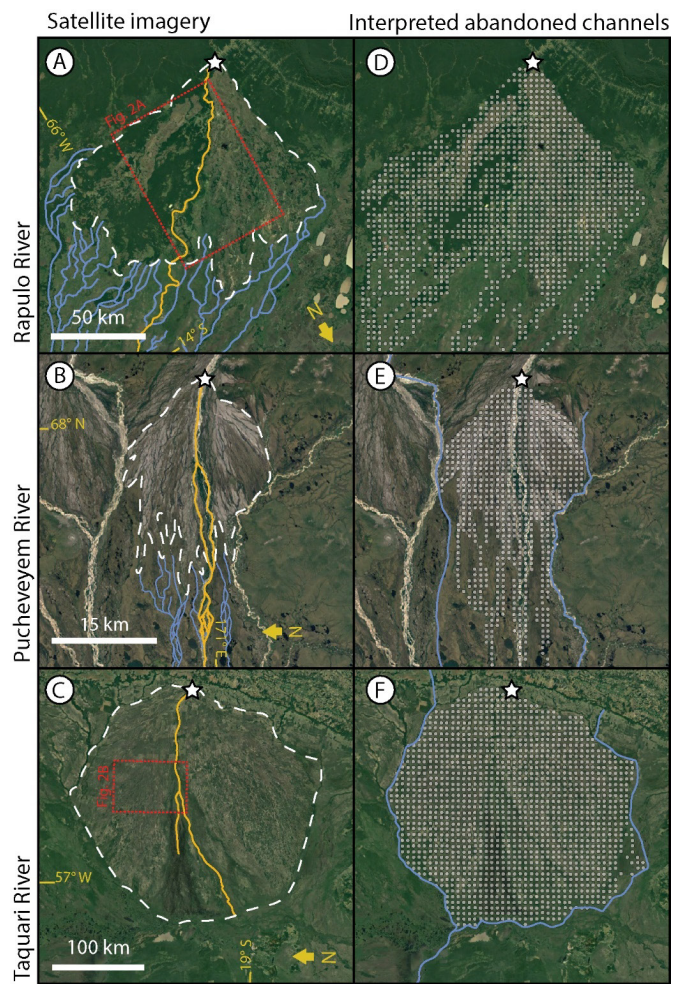
117 While little is known about the constructive and destructive processes in action on floodplains, we can speculate on
118 the evolution of abandoned channels using observations from both degradational and aggradational settings (Hartley et al.,
119 2010b).

120 There is field evidence that abandoned channels heal. During floods, overbank sediments can preferentially deposit
121 in abandoned channel topographic lows (Wolman and Eiler, 1958; Schmudde, 1963; Bridge and Leeder, 1979; Lewis and
122 Lewin, 1983; Farrell, 1987; Nanson and Croke, 1992; Tooth et al., 2002; Jerolmack and Paola, 2007). This healing, however,
123 can be undone in some cases by scouring from future flooding events (Wolman and Leopold, 1957; Wolman and Eiler, 1958;

124 Schmudde, 1963; Bridge and Leeder, 1979). What happens to abandoned channel highs, on the other hand, is not well
125 understood. The relative degree of levee erosion or deflation (something we call 'top-down' healing) is unknown. Top-down
126 healing is plausible if a combination of diffusive sediment transport, weathering, and fluvial erosion during floods erode or
127 diffuse topographic highs on the floodplain (Hack and Goodlett, 1960; Burkham, 1972; Zwoliński, 1992; Gabet, 2000; Croke
128 et al., 2013). High elevation on floodplains could conceivably be eroded during subsequent flood events, or could conceivably
129 be gradually diffused; similar to hillslopes (Roering et al., 1999), beawhileuse While floodplain slopes are characteristically
130 low, biologic disturbance is often high. That said, it is not clear whether diffusion should also describe the evolution of
131 alluvial floodplain topographic highs, biologic disturbance is often high (Richards et al., 2002; Steiger et al., 2005).
132 Complicating matters, sediment deposition during overbank flows has also been observed atop flat or even positive floodplain
133 topography, promoting self-sustaining topography that also hinders abandoned channel healing (Jahns, 1947; Wolman and
134 Eiler, 1958; Schmudde, 1963; Nanson, 1980).

135 In summary, there are unanswered questions about the fates and rates of abandoned channel floodplain topography.
136 There are virtually no data that describe how these landforms change through time once they are abandoned on the floodplain.
137 This is an important knowledge gap because the primary mode of sediment transport and emplacement in this depositional
138 environment is via alluvium deposited by and between avulsions. It is conceivable that the gross morphology of foreland basins
139 and their deposits depends on the interaction between avulsing rivers and abandoned channels. To motivate this idea further
140 we show in the next section that modern megafans are covered with abandoned channels.

141



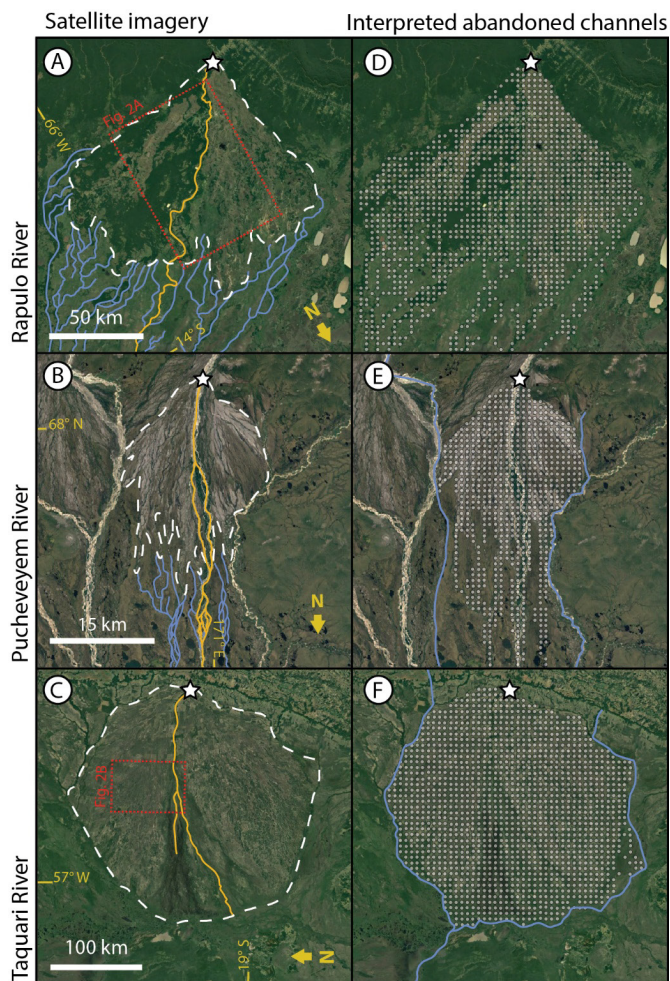


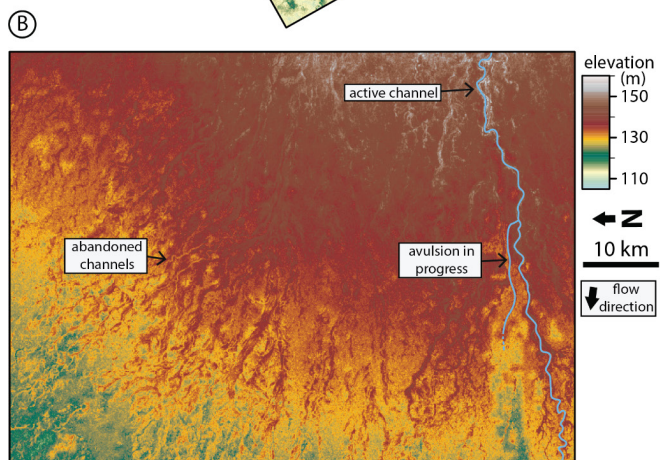
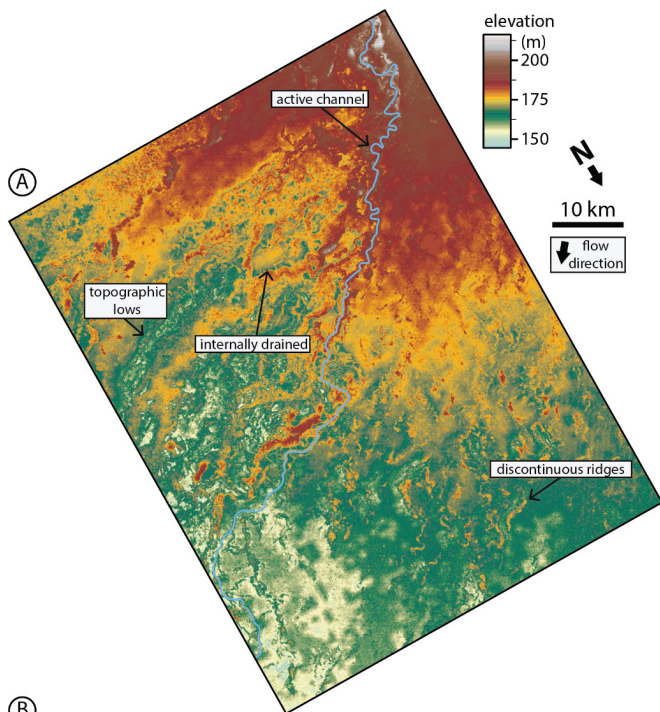
Figure 1: (a-c) Remote sensing images and (d-f) abandoned channel maps for three fluvial megafans. The fans are located along the Rapulo River in Bolivia (a,d), the Pucheveyem River in Russia (b,e), and the Taquari River in Brazil (c,f). Note the downstream transition between distributive, densely channelized abandoned channel networks to tributive, sparsely channelized networks. Dashed white lines in (a-c) are interpreted megafan boundaries (see text for details), and white stars mark megafan apices. Blue lines in (a-c) show interpreted abandoned channel pathways outside of the megafan boundary. Solid gold lines show active channels. All satellite images are USGS/NASA Landsat/Copernicus, © Google Earth.

23. Observations of modern fluvial megafan surfaces

In order to motivate considering the importance of abandoned channels on avulsion dynamics, we must ~~WTe~~ investigate the pervasiveness of abandoned channels in landscapes where avulsions are common. To do this, we created maps of abandoned channels on a non-exhaustive set of three megafans (Fig. 1) that represents a range of megafan sizes and settings with typical appearances (Hartley et al., 2010a; Weissmann et al., 2010). ~~This set incl. and that includes~~ the well-studied Taquari megafan (e.g., Assine, 2005; Makaske et al., 2012; Zani et al., 2012). Following previous work (Rossetti and Valeriano, 2007; Bernal et al., 2011), we combine Google Earth, Landsat visual imagery, and bare-earth topography to identify abandoned channels on ~~South American~~~~these~~ megafans. For elevation data, we use the BEST (Bare-Earth Srtm Terrain) elevation model, which uses vegetation maps and satellite lidar to reveal bare-earth topography by correcting for vegetation elevations present in radar-derived topography (O'Loughlin et al., 2016; Moudrý et al., 2018). On top of each megafan, we overlaid a rasterized grid with square cells with dimensions that corresponded to roughly five channel widths, similar to the resolution of the cellular model that is described later. Within each cell we marked whether there was topographic or visual evidence of abandoned channels (Fig. ~~1B~~1D-F). Evidence of abandoned channels consisted of identified channelized features with long axes generally oriented toward the apex of the fan, with widths approximately equal to the active channels on the fan. Abandoned channels were usually visible in satellite imagery, but in areas with dense tree canopies, we looked for channel-like pathways delineated by differences in coloration against the adjacent floodplain. These differences result from the historical presence of an active channel (Bernal et al., 2011); abandoned channels may have coloration that is lighter (due to sediment emplacement; Valenza et al., 2020) or darker (due to increased vegetative density associated with additional standing or groundwater). Where possible, we used the topographic data in tandem with the visual data to confirm that a cell contained an abandoned channel.

23.1. Remote sensing results:

These three fluvial megafans have abundant abandoned channels within their boundaries (Fig. 1). Megafan boundaries were drawn to encapsulate regions of positive relief and greater slope relative to the surrounding basin (~~dashed white lines~~, Fig. 1A-C). Within these boundaries, between 95% (Rapulo) and >99% (Pucheveyem and Taquari) of cells on megafan surfaces contained interpreted abandoned channel features. Downstream of the megafan boundary there is a transition from distributive to tributive planform morphologies (Fig. 1A,B), wherever they are not bounded by topography or an axial river (Fig. 1C; cf. methodology of Hartley et al., 2010a). In contrast to other distributary fan systems like alluvial fans or some deltas, within the fan we usually observed a single active channel with one or multiple threads and occasional bifurcation (Hartley et al., 2010a). This suggests that, rather than hosting many contemporaneous distributary channels, the distributive nature of megafans arises over time through repeated avulsions along a small number of active channels (Weissmann et al., 2010).



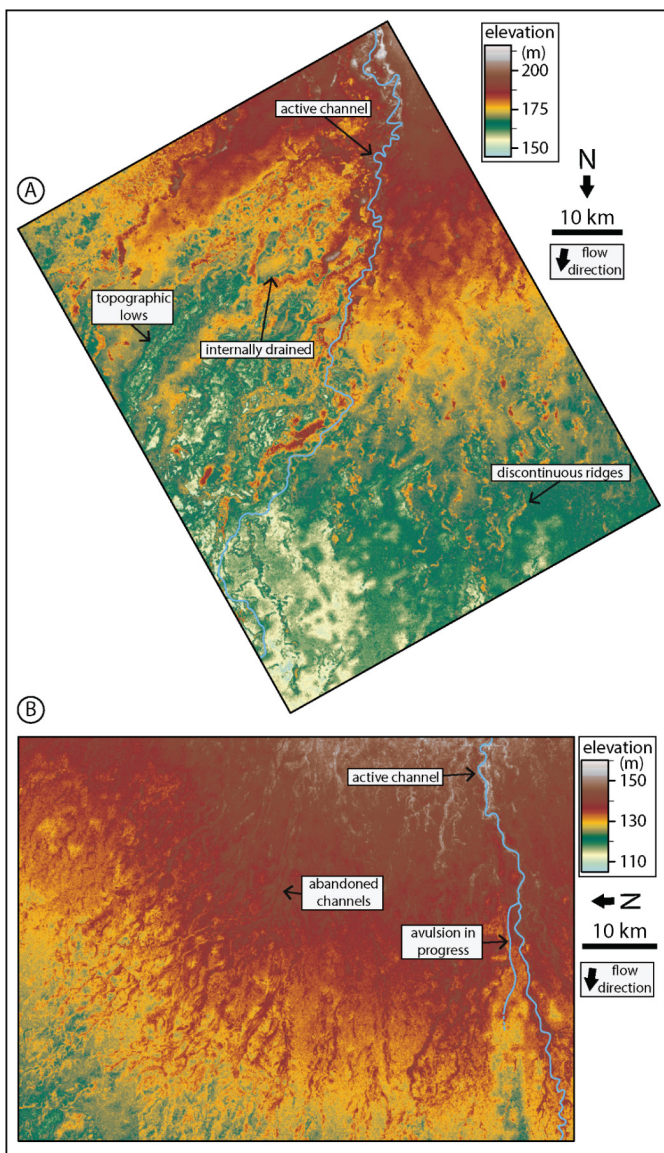


Figure 2: Bare-earth digital elevation models (O’Loughlin et al., 2016) of floodplain topography on the Rapulo (a) and Taquari (b) megafans. Locations are in Fig. 1. Floodplains are densely channelized by abandoned channels with visible topographic highs and lows corresponding to levees or alluvial ridges and channel beds, respectively. Note the presence of discontinuous alluvial ridges. Also note that the colorbar used is not perceptually uniform, meaning that small changes in certain elevations ranges are highlighted more drastically than others, especially in the red-yellow band of this image; this is done to emphasize low-relief features relative to the overall fan slope necessary as abandoned channels are low-relief features relative to the overall slope of megafans.

We observed that abandoned channels can be both topographic highs (associated with levees or alluvial ridges) and topographic lows (associated with abandoned channels that have not been fully in-filled with sediment) relative to surrounding floodplains (Fig. 2). In some portions of the fan there were ‘internally drained’ areas surrounded by topographic abandoned channel highs (Fig. 2A). These abandoned alluvial ridges were not necessarily spatially continuous in the downstream direction, often forming discontinuous ridges (Fig. 2; Rossetti and Valeriano, 2007). The topographic data were collected during an ongoing avulsion on the Taquari fan, and the avulsion location is immediately adjacent to a topographic low on its floodplain (Buehler et al., 2011). Multiple avulsions on the Rapulo megafan during the Landsat observation period have also initiated into local topographic lows adjacent to the channel (Edmonds et al., 2022).

2.3.2. Megafan floodplain topography discussion:

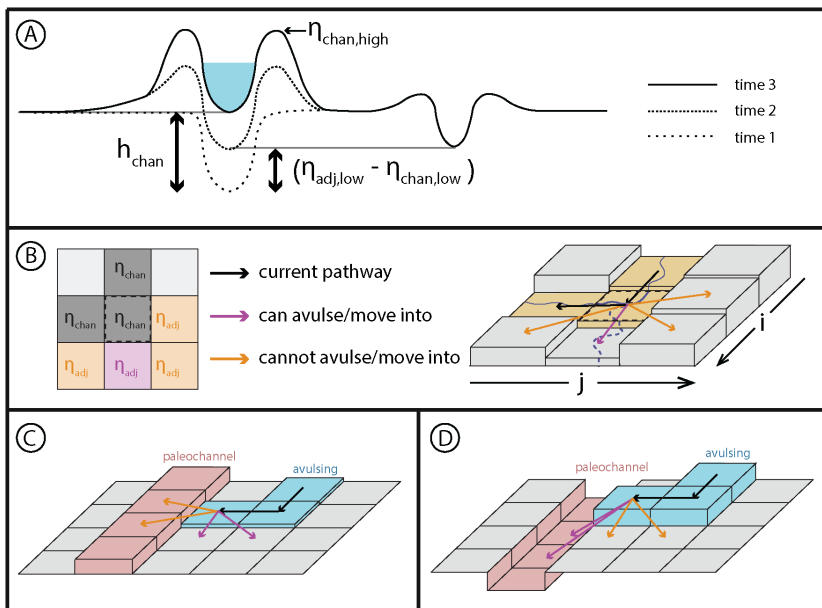
The degree of floodplain channelization observed and interpreted on megafan surfaces in Fig. 1 and Fig. 2 compares well to the model results of Jerolmack and Paola (2007) and Reitz et al. (2010), and suggests that most avulsions would should be influenced by interact with abandoned channels. Following this, we envision at least two aspects of avulsion dynamics that can be influenced by the presence of abandoned channels and can be easily incorporated into a model.

2.3.2.1 Avulsion set-up & initiation

The most common conception of avulsion set-up is superelevation, whereby in-channel deposition outpaces deposition in the surrounding floodplain, leading to a perched channel that transports water and sediment less efficiently than some novel path on the floodplain (Bryant et al., 1995; Slingerland and Smith, 2004). On a flat, featureless floodplain where subsidence is uniform along-strike with a channel that can counter-act subsidence exactly, the time to achieve superelevation (T_A , years) for some arbitrary point along a river is commonly (e.g., Jerolmack and Mohrig, 2007; Jerolmack, 2009; Martin et al., 2009; Reitz et al., 2010; Moodie et al., 2019) approximated as

$$T_A = \frac{\beta * h_{chan}}{(A_{chan} + \sigma) - A_{fp,tot}} \quad (1)$$

where β is a non-dimensional channel depth fraction (generally assumed to be 0.5-1.0; Mohrig et al., 2000), h_{chan} is the channel depth (meters) at a particular point in the river, A_{chan} is the in-channel-bed aggradation rate (meters per year), $A_{fp,tot}$ is the total floodplain aggradation rate (meters per year), and σ is the subsidence rate (meters per year, positive in the downwards direction). Conceptually, this superelevation timescale is equal to the time necessary for the channel bed to aggrade some specified fraction of a channel depth (Fig. 3A).



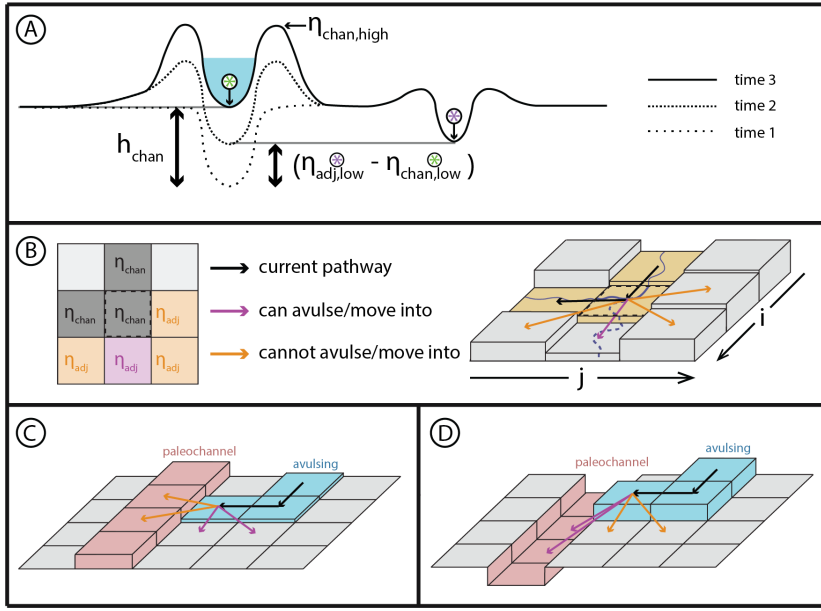


Figure 3: (a) Conceptual understanding of avulsion set-up by superelevation, and how the magnitude of in-channel aggradation necessary to achieve aggradation (black bidirectional arrows) differs if abandoned channels are ignored (left of active channel; Eq. (1)) or considered (right of active channel; Eq. (2)). (b) Representation of avulsion set-up by superelevation in a 2D cellular setting that considers adjacent elevations. Cells in the left panel are marked as η_{adj} if they are adjacent to the center cell, highlighted by the dashed black line in the left and right panels. In this case, the cell is superelevated and enjoys a gradient advantage to only one other cell (immediately downdomain) and can thus avulse into this cell. The subscript “low” applies to all labeled cells but is omitted for legibility. Model representation of (c) abandoned channel repulsion and (d) attraction.

Abandoned channels on the floodplain can short-circuit this timescale by reducing the amount of aggradation needed to superelevate (Fig. 3A). If an abandoned channel is close to the active one, then this should encourage avulsion because during high flow there would be a steep water surface gradient that would cause erosion of the intervening levee and reroute the flow. This requires that the abandoned channel is roughly the same size as the active one and that it is close enough to increase the water surface gradient. What constitutes ‘close enough’ is unknown, though the Taquari avulsion is observed to proceed into an adjacent topographic low (~1 km from the parent channel; Fig. 2B), as are repeated avulsions along the Rapulo river (Edmonds et al., 2022). In effect, the lower elevation of the abandoned channel bed relative to its surrounding floodplain reduces the amount of aggradation needed for superelevation. We can thus rewrite the superelevation timescale of Eq. (1) as

$$T_A = \frac{\beta * (\eta_{adj,low} - \eta_{chan,low})}{A_{chan}(A_{chan} + \sigma) - A_{fp,tot}}, \text{ for } \eta_{adj,low} > \eta_{chan,low} \quad (2)$$

where $\eta_{chan,low}$ and $\eta_{adj,low}$ represent the elevations (meters) of the active channel bed and the area adjacent to the channel, respectively (Fig. 3A,B). This adjacent elevation can vary based on the topography adjacent to the channel. For example, if there is an abandoned channel bed that is inset into the surrounding floodplain adjacent to the river, then the active channel becomes superelevated relative to the abandoned channel when $\eta_{chan,low} = \eta_{adj,low}$. When this difference ($\eta_{chan,low} - \eta_{adj,low}$) $\eta_{adj,low} - \eta_{chan,low} < h_{chan}$ (see Fig. 3A), and then Eq. (2) will result in a shorter avulsion set-up timescale than would be expected for a featureless floodplain (Eq. (1); Mohrig et al., 2000). Even though this is a simple amendment to Eq. (1), as we show later it has important effects on avulsion timing and location.

Channel reoccupation could also shorten superelevation timescales. Given the density of channels we observed on megafans (Fig. 1; Fig. 2), and observations from the stratigraphic and remote sensing records, it seems that reoccupation must be common (e.g. Mohrig et al., 2000; Chamberlin and Hajek 2015, 2019; Valenza et al., 2020). When active channels avulse, any previous aggradation downstream of the avulsion locus is not immediately destroyed. Instead, if these channels are later reoccupied, and had not been completely scoured out in the interim, then Eq. (2) allows for superelevation to be inherited. In these two ways, abandoned channels can cause rivers to have avulsion set-up timescales that are much less than via relative aggradation or subsidence alone as embodied in Eq. (1).

2.2.2 Avulsion pathfinding

Abandoned channels are so prevalent on fan surfaces that they should also affect avulsion pathfinding (Fig. 1; Fig. 2; Edmonds et al., 2016; Valenza et al., 2020). Despite this, most previous models have assumed abandoned channels have no effect on future avulsion pathfinding (Leeder, 1977; Ratliff et al., 2018), or act as universal repulsors (Allen, 1978; Bridge and Leeder, 1979) or universal attractors (Sun et al., 2002; Jerolmack and Paola, 2007; Reitz et al., 2010). The reality seems to be somewhere in between these endmembers. After all, if abandoned channels retain superelevation that once drove avulsion and abandonment, then that superelevation would topographically repel later pathfinding events (Leeder, 1977; Allen, 1978; Fig. 3C). We observe both topographic lows and highs on modern megafans, including discontinuous alluvial ridges (Fig. 2). This suggests that abandoned channels can be both attractive and repulsive at different locations and times on the fan surface (Allen, 1978). This is consistent with recent observations that suggest avulsions are pushed away from their parent channels by alluvial ridges but inevitably attracted back into a channel some distance downstream (Edmonds et al., 2016; Valenza et al., 2020). Importantly, attraction seems to be a near universal behavior; all 63 avulsions identified by Valenza et al. (2020) experienced some reoccupation.

In addition to affecting avulsion dynamics, the rate at which these abandoned channels (and associated alluvial ridges and scours) are removed should affect landscape evolution because abandoned channels contribute much or most of the topography on modern megafans (Fig. 2). There are virtually no observations of abandoned channel healing rates, and as such

it is unclear in models whether to treat abandoned channels as healing instantly, persisting indefinitely, or some intermediary. Additionally, if one assumes that abandoned channels do heal, the mode of abandoned channel healing is unclear; while preferential deposition in abandoned channel topographic lows ('bottom-up' healing) is known to occur in at least some abandoned channels (Schmudde, 1963; Toonen et al., 2012), the relative degree of levee erosion ('top-down' healing) is unknown. Top-down healing is plausible if a combination of diffusive sediment transport, weathering, and fluvial erosion during floods erode topographic highs on the floodplain (Haack and Goodlett, 1960; Burkham, 1972; Zwoliński, 1992; Gabet, 2000; Croke et al., 2013). See Sect. 5.2 in the Discussion for more details. In summary, however, there are unanswered questions about the fates and rates of abandoned channel floodplain topography. These questions have important implications for the gross morphology of foreland basins and their deposits because the primary mode of sediment transport and emplacement in this depositional environment is via alluvium deposited by and between avulsions.

34. Model conception and implementation

34.1 Model overview & routine

The prevalent channelization of fluvial megafan surfaces led us to consider how abandoned channels may affect avulsion dynamics and landscape evolution in foreland basin settings. To test these effects, we created a physically based cellular model of an evolving alluvial landscape with parameterized and tuneable abandoned channel dynamics ('RiverWalk'; available at DOI:10.5281/zenodo.5576789). Our model is intentionally simplified as much as possible while retaining the ability to recreate the essential features of fluvial megafans in foreland basins (Bokulich, 2013). As a brief conceptual overview, our model consists of a single river exiting a mountain-front and transporting some fixed amount of water discharge and sediment flux. As it enters a foreland basin, relative subsidence (~~high near the mountain front, decreasing -and decreases linearly into the basin~~) causes sediment to be deposited preferentially near the mountain-front. This leads to river avulsion via superelevation, and over time these avulsions construct a radially oriented fan through the emplacement of channels that individually aggrade before abandonment. In our model, these abandoned channels can affect avulsion dynamics. For simplicity, we ignore the impacts of other rivers or fans and of any other mountain-front processes that may advect sediment into the basin. ~~The sensitivity of the model to model is generally insensitive to small changes in most -in external, non-experimental parameters is explored below in (section Sect. 5.6.1 of the Discussion).~~

The model routine operates as follows; more details on individual components are provided in Tables 1 and 2 and in the sections that follow. We paired a 1D diffusive channel-bed-elevation model (Paola et al., 1992) that describes how elevation in a river channel diffuses due to sediment transport with a rectangular, 2D cellular computational domain of 150 km per side that describes the floodplain and surrounding basin. Following Jerolmack and Paola (2007), each cell has a low (channel-bed) and high (levee or alluvial ridge) elevation. The simulation initializes by assuming the channel takes a straight path to the bottom of the domain (Table 1). The 1D sediment transport model is calculated to equilibrium along this path (Table 1). This profile is then ~~replicated along strike to populate~~ used to populate floodplain cells by setting the elevation of every floodplain

296 [cell equal to the equilibrium elevation an equal distance from the mountain-front along this path](#). This creates an underfed
297 basin because nearly all subsequent river paths will be longer than a straight line, which causes aggradation and avulsion.
298

299
 300 **Table 1: Non-experimental Cellular avulsion model parameters. Values for parameters were not chosen to bemodel any specific river**
 301 **or megafan, but rather as reasonable representative values that resulted in the formation of a generic system that is representative**
 302 **of rivers commonly found atop megafans in mountain-front regions, including those seen in Figure 1.**

Parameter	Value
Timestep	10 yr
Grid Dimensionsdimensions	301 cells x 301 cells
Cell Sizesize	500 m x 500 m
Random Walkwalk Weightsweights	In descending order of steepness: 40%, 27.5%, 17.5%, 10%, and 5%
Minimum Superelevation—superelevation (β sensu Mohrig et al., 2000.)	Channel-base equal to neighboring floodplain cell ($\beta = 1$)
Overbank Aggradation—aggradation (Fixed-base Rate Component; $A_{p,fbase} - A_{p,s}$)	Upstream boundary: 2×10^{-7} m/yr Downstream boundary: 5×10^{-6} m/yr 2.55×10^{-6} m/yr
Subsidence Rate—rate (linearly interpolated; σ)	Upstream boundaryProximal: 1×10^{-5} m/yr Downstream boundaryDistal: 5×10^{-6} m/yr
Initialization Lengthlength	Variable; Set such that initial apex elevation is ~5-10% less than final apex elevation; see Table 3

303
 304 After the first avulsion, a new river pathway is established within a single timestep from the avulsion point (Sect.
 305 34.3.1) and is set into the domain one channel depth below the surface. The pathway is selected via steepness-weighted random
 306 walk to any point along the bottom boundary of the domain (Sect. 34.3.1), and all floodplain cells along this path are converted
 307 to active channel cells (Sect. 34.3). The timestep increments and the elevations of each cell along the new pathway are
 308 transiently diffused to represent river adjustment (Sect. 34.3). At the upstream boundary of the diffusion model, water and
 309 sediment come in at a fixed rate so that the surface slope does not change (Table 2), and at the downstream boundary the
 310 channel-bed elevation is fixed at 0 m. Diffusion continues until an avulsion trigger (with a fixed probability at each timestep)
 311 occurs and avulsion criteria (superelevation and gradient advantage) are satisfied for at least one active channel cell (Sect.
 312 34.3.1). The avulsion location is randomly selected from among viable cells and pathfinding proceeds as before, but now the
 313 river can be repelled or attracted (i.e., captured) by abandoned channels. Pathfinding stops when the avulsion is successful and
 314 encounters the bottom boundary, or when the avulsion fails after becoming terminally trapped (Sect. 34.3.1). In both situations
 315 the timestep is incremented, but in the successful case any active channel cells that are no longer occupied become abandoned
 316 channel cells, and in the failure case the domain is restored to its pre-avulsion state.
 317

Formatted: Justified, Indent: First line: 0.5", Line spacing: 1.5 lines

318 Table 2: Sediment diffusion calculation parameters.

Parameter	Value
Initial Specific-specific Discharge-discharge (apex)	1.9 x 10 ⁵ m ² /yr
Incoming Sediment-sediment Supplysupply	400 m ³ /yr
Basin Width-width (for discharge calculation)	5 x 10 ⁴ m
Coefficient A	1.00
Nondimensional coefficient of friction	0.01
C_0	0.7
S	1.65
$\rho_{sediment}$	2.65 x 10 ³ kg m ⁻³
ρ_{water}	1.00 x 10 ³ kg m ⁻³

319

320 In all future timesteps, after updating the 2D landscape and before checking for avulsion triggers, floodplain and
321 abandoned channel processes routines are executed. First, cells experience subsidence at a rate that decreases away from the
322 mountain front (representing a foreland basin) and overbank floodplain deposition that varies with distance from the mountain
323 front but not with distance from the channel (Sect. 3.4.3.2). Next, abandoned channels are healed by a steady-rate topographic
324 adjustment function until they reach a specified healing endpoint (3Sect. 4.3.2). Finally, any abandoned channel cells with less
325 than 25% of a mean channel depth in remnant relief are converted to floodplain cells (Sect. 3.4.3).

326 **3.4.2 1D diffusive channel-bed elevation model**

327 The 1D model has a variable length that is equal to that of the planform river pathway established in the 2D model.
328 We used transient diffusion to model channel-bed elevation changes along this pathway that would occur from sediment
329 transport (Paola et al., 1992):

330
$$\sigma + \frac{\partial \eta_{chan,low}}{\partial t} = \frac{\partial}{\partial x} \left(v \frac{\partial \eta_{chan,low}}{\partial x} \right), \quad v = - \frac{8qA\sqrt{c_f}}{C_0(S-1)} \quad (3)$$

331 where t is time (years), x is space (meters), v is diffusivity (square meters per year), q is normalized water discharge per unit
332 basin width (square meters per year), A is a non-dimensional constant set to 1, c_f is a dimensionless drag coefficient, C_0 is bed
333 sediment concentration, and S is sediment specific gravity ($\frac{\rho_{sediment} - \rho_{water}}{\rho_{water}}$, non-dimensional; Table 2). We used the Crank-
334 Nicolson solution scheme to solve this equation. This scheme is second-order, implicit in time, and unconditionally
335 numerically stable for diffusion partial differential equations (Slingerland and Kump, 2011). Treating diffusion of the bed
336 surface transiently (rather than bringing the river completely to equilibrium between each timestep [cf. Jerolmack and Paola,
337 2007]) allows for local aggradation or incision to occur on channel profiles out of equilibrium.

338 Our experimental design necessitated using nondimensional repulsion and attraction factors that are normalized to
339 channel depths. As such, it was necessary to determine channel depth (h_{chan}) for each active channel cell. We solved for this
340 at every active channel cell once per timestep following Paola et al. (1992; Table 2). This method allows depth to vary as a
341 function of local slope. Immediately after avulsion, slope variations along channels can be extreme (Fig. 8). These extreme

variations in slope create unrealistic variations in depth over short distances. As such, when solving for channel depth, we bound maximum and minimum slope to within a factor of two compared to the equilibrium profile.

34.3 2D cellular model: avulsions and floodplains

The computational domain is discretized into square cells of length 500 m. There are three types of cells in our model: active channel ($chan$), abandoned channel ($aban$), and floodplain (fp). All cells have two elevations ('high' and 'low') that we track throughout each run. All elevations are measured in meters.

Active channel: Active channel cells represent the current pathway of the river. There is one contiguous pathway for flow per timestep. We selected a cell size such that modeled rivers are approximately one fifth of the width of a cell; as a result, channel-scale processes (like meandering, crevasse splays, or other lateral-distance-dependent depositional effects) are not resolved.

The low elevation in each active channel cell represents the channel bed and is updated by transient diffusion as described in Eq. (3). Then, high elevations are set to the greater of i) the high elevation at the last timestep, or ii) one channel depth above the bed, such that:

$$(\eta_{chan,low})_t \text{ is given by Equation 3} \quad (4a)$$

$$(\eta_{chan,high})_t = \max \left\{ (\eta_{chan,high})_{t-1}, (\eta_{chan,low})_t + h_{chan} \right\} \quad (4b)$$

where t is the current timestep and $t - 1$ is the prior one. This assumes that an aggrading river constructs levees that can contain its flow depth, but levees are not lowered if the river incises.

Other cell types become active channel cells whenever they are occupied by the active channel after an avulsion. During this process, the low elevations of the new channel pathway are inset one channel depth down from the high elevations unless there is a channel that is already incised beyond this depth. This rule allows for channels to inherit levees (and superelevation) and does not further erode abandoned channel cells that are already incised more than one channel depth below their levees.

Abandoned channel: Abandoned channel cells include any cell that was once active but no longer contains water. These cells are still capable of attracting and repulsing pathfinding avulsions. Each cell has low and high elevations that reflect abandoned channel beds and levees, respectively. These elevations experience a linear healing rate that depends on healing mode but ultimately adjusts the channel bed and levee elevations toward a specified endpoint (Sect. 34.3.2):

$$\eta_{aban,low} = (\eta_{aban,low})_{t-1} + (A_{fp,tot} - \sigma) + H_{low} \quad (5a)$$

$$\eta_{aban,high} = (\eta_{aban,high})_{t-1} + (A_{fp,tot} - \sigma) + H_{high} \quad (5b)$$

where $A_{fp,tot}$ is the total overbank aggradation rate on the floodplain (meters per year; Sect. 34.3.2), and H_{low} and H_{high} are the healing rates (meters per year) applied to the low and high elevations, respectively.

372 Abandoned channel cells can become active channel cells if they are later occupied after an avulsion. Otherwise, they
 373 will become floodplain cells when:

$$374 \quad h_{aban} < (0.25 * \bar{h}) \quad (6a)$$

$$375 \quad h_{aban} = (\eta_{aban,high} - \eta_{aban,low}) \quad (6b)$$

376 where \bar{h} is mean channel depth (meters) calculated over the entire length of the active channel at each timestep. While healing
 377 gradually lowers h_{aban} , there is no process that can increase this relief other than revisitation by the active channel, in which
 378 case the cells will become active channel cells.

379 Floodplain: Floodplain cells are those never been visited by a channel or have completely healed after visitation. High
 380 and low elevations are equal for floodplain cells except if they were once abandoned and have transitioned to floodplain (via
 381 the threshold in Eq. (11)) they maintain their unequal elevations until healing is complete. Floodplain cells do not repulse or
 382 attract pathfinding avulsions. However, their remnant (and possibly unequal) elevations do affect set-up and avulsion
 383 pathfinding via weighted random walk (Sect. 34.3.1).

384 Floodplain cells that retain any remnant relief are subjected to healing in the same manner as abandoned channel
 385 cells:

$$386 \quad \eta_{fp,low} = (\eta_{fp,low})_{t-1} + (A_{fp,tot} - \sigma) + H_{low} \quad (7a)$$

$$387 \quad \eta_{fp,high} = (\eta_{fp,high})_{t-1} + (A_{fp,tot} - \sigma) + H_{high} \quad (7b)$$

388 34.3.1 Avulsion processes:

389 Avulsion set-up: Avulsions occur via three steps: i) set-up, ii) initiation via triggering, and iii) floodplain pathfinding.
 390 Avulsion set-up (Slingerland and Smith, 2004) occurs from a combination of superelevation and flowpath gradient advantage.
 391 A cell is superelevated if the elevation of its channel-bed is equal to or greater than at least one of its five neighboring cells
 392 (not including the three upstream cells; Fig. 3A,B) by some fraction of a mean channel depth:

$$393 \quad (\eta_{chan,low} - \eta_{adj,low}) \geq (\beta - 1) * \bar{h} \quad (8)$$

394 We set $\beta = 1$, which requires the active channel bed to meet or exceed an adjacent cell's low elevation (Mohrig et al.,
 395 2000). As such, cells are considered superelevated when:

$$396 \quad (\eta_{chan,low} - \eta_{adj,low}) \geq 0 \quad (9)$$

397 Our results are insensitive to values of β between 0.5 and 1. In addition to superelevation, an avulsion in our model
 398 must have a local gradient advantage over its previous pathway. We calculate this gradient over the first step into surrounding
 399 cells-of-each-flow-path, as opposed to over the entire pathway (cf. Ratliff et al., 2018).

400 Avulsion triggering: Once a portion of a river is superelevated, some triggering event is necessary to initiate a
 401 avulsion. Predicting natural triggers is challenging because they can take the form of floods, ice damming, bank erosion, woody
 402 debris dams, neotectonics, meander bend cutoffs, beaver dams, bar migration, or other events that allow flow to escape normal
 403 channel confinement (Harwood and Brown, 1993; Smith et al., 1998; Ethridge et al., 1999; Jones and Schumm, 1999; Mohrig

Formatted: Indent: First line: 0.5"

et al., 2000; Slingerland and Smith, 2004; Gibling et al., 2010; Morón et al., 2017). With that said, we know that trigger recurrence can only be as long as observed avulsion periods in natural river systems, which range from 10^1 years on the Kosi River megafan to 10^3 years on the Mississippi delta (Wells and Dorr, 1987; Aslan et al., 2005; Jerolmack and Mohrig, 2007). We set an average avulsion trigger period of 30 years by specifying a fixed probability of a trigger occurring on any given timestep. We select 30 years as it provides ample opportunity for a river to avulse, provided avulsion set-up criteria are met. Since triggers cannot initiate avulsions in the absence of set-up via superelevation (Slingerland and Smith, 2004), this effectively sets a lower limit on avulsion period, but the actual period may be longer if there are no superelevated river segments along the active channel when a trigger occurs.

Avulsion pathfinding: Whenever an avulsion trigger occurs, avulsion pathfinding initiates from a randomly selected active channel cell that meets the set-up criteria. From here, the new channel path follows a steepness-weighted random walk if it remains in floodplain cells. Each step, the pathfinding avulsion can move into one of five cells (three downstream and two lateral). The cell is selected randomly, and the choices are weighted by steepness (see Table 1 for weighting scheme). Model outcomes are not sensitive over reasonable ranges of steepness weights, so long as all five directions are possible. The river is prevented from returning to its previous position and movement beyond the domain boundaries.

When a pathfinding avulsion is adjacent to an abandoned channel cell, the model checks to see if the abandoned channel cell is repulsive or attractive (Fig. 3C,D). Abandoned channel cells are repulsive when their levee heights above the adjacent floodplain (L_h ; meters) are larger than some multiple of the pathfinding avulsion flow depth (h_{avul} ; meters):

$$L_h > \alpha_R * h_{avul} \quad (10a)$$

$$L_h = (\eta_{aban,high} - \eta_{appr,low}) \quad (10b)$$

where α_R is a nondimensional repulsion factor, h_{avul} is the threshold channel depth calculated with diffusion theory (Paola et al., 1992) assuming the flow is channelized during pathfinding, and $\eta_{appr,low}$ is the low elevation in the adjacent cell from which the pathfinding avulsion channel approaches the abandoned channel. α_R is a threshold for how tall levees must be to repulse advancing flow. Lower values are more repulsive since the threshold to repel is lower. A value of zero means that any positive value of L_h would cause repulsion.

Abandoned channel cells are attractive when h_{aban} (meters) is larger than some fraction (α_A) of mean flow depth:

$$h_{aban} > \alpha_A * \bar{h} \quad (11)$$

α_A is a threshold value describing how much remnant relief an abandoned channel must retain to capture flow. Lower values are more attractive since ~~the threshold it means only a small fraction of the average original channel relief is required to be attractive-to-attract-is lower.~~ If captured, the pathfinding avulsion will move in the direction of the lowest $\eta_{aban,low}$. This will continue unless there are no abandoned channel cells into which flow can proceed, which can happen if the abandoned channel is discontinuous (Fig. 2), in which case the river is ejected back onto the floodplain and resumes steepness-weighted random walk.

Rivers that are repulsed or not captured by abandoned channels will proceed via steepness-weighted random walk until they exit the domain. If during pathfinding there are no viable moves, which can happen within floodplains bounded by abandoned channels that cannot be reoccupied (Fig. 2), the avulsion fails, and all cells are reverted to their pre-avulsion states, and the model increments to the next timestep. This While this implementation of failed avulsion pathfinding is a simplification, but it conceptually reflects healed crevasse splays (Slingerland and Smith, 2004) and matches limited observational evidence, including among avulsions on the Rapulo river (Edmonds et al., 2022).

34.3.2 Floodplain processes:

Floodplain processes are applied to all abandoned channel and floodplain cells. These processes include rules for 1) overbank deposition; 2) subsidence; and 3) abandoned channel healing.

Floodplain deposition & subsidence: We implement an overbank deposition rate that is constant along grid rows. As channels are considered small relative to the width of a cell, there is now we assume that any distance-from-channel-dependent component to overbank sedimentation is contained within a single cell (cf. Bridge and Leeder, 1979; Pizzuto, 1987). Instead, and similar to Jerolmack and Paola (2007), the total floodplain aggradation for each row ($A_{fp,tot}$; meters per year) is described by a depth-dependent variable rate the product of a base rate ($A_{fp,base}$, meters per year) that and an additional term that increases linearly with the vertical distance between the highest elevation ($\eta_{high,max}$) in that row and the elevation of a far-field floodplain cell that has never been visited by the active channel ($\eta_{farfield}$). While simple, this depth-dependent scaling reflects a basic intuition that regions of the basin that are inundated to a greater depth beneath the highest levee (often the active channel) during flooding should receive more overbank sediment. The vertical distance term is nondimensionalized by dividing by mean channel depth as averaged over the entire active channel. The base rate $A_{fp,base}$ increases downstream, described by a linear interpolation between an upstream and downstream boundary value, and reflects an intuition of a river increasing in suspendable sediment (e.g., washload) downstream. This vertical distance is normalized to units of mean channel depth as averaged over the entire active channel. While simple, this scaling reflects a basic intuition that regions of the basin that are inundated to a greater depth beneath the highest levee (often the active channel) during flooding should receive more overbank sediment. Finally, we assume that total overbank deposition on the floodplain ($A_{fp,tot}$) cannot exceed subsidence (σ , meters per year) so that the surface does not rise over time:

$$A_{fp,tot} = \min \left\{ A_{fp,base} * \frac{\eta_{high,max} - \eta_{farfield}}{\bar{h}}, \sigma \right\} \quad (12)$$

Equation (12) deposits equal amounts of sediment on abandoned channel lows as highs, and thus does not heal abandoned channels over time. Healing is instead handled separately and described in the following section. Finally, as a basic approximation of foreland basin style subsidence, we apply subsidence at each timestep at constant rates. These rates vary spatially via linear interpolation between a pair of rates representing proximal and distal values, with the proximal rates being two times greater.

467 Abandoned channel healing: Despite the critical importance that floodplain topography and abandoned channel
 468 healing timescales play in affecting channel network evolution in avulsing systems (Jerolmack and Paola, 2007; Reitz et al.,
 469 2010), there is no consistent choice of rules for implementing this phenomenon in models of avulsion. ~~See the Discussion for~~
 470 ~~a more comprehensive review of abandoned channel implementation in avulsion models.~~ In our model, we implemented
 471 different abandoned channel healing styles to explore how they influence avulsion dynamics and landscape evolution. Within
 472 these styles, abandoned channels can be healed 'bottom-up' as they are filled with sediment, have 'top-down' as their levees
 473 are eroded, or have both elevations adjusted toward the far-field floodplain (Fig. 4).

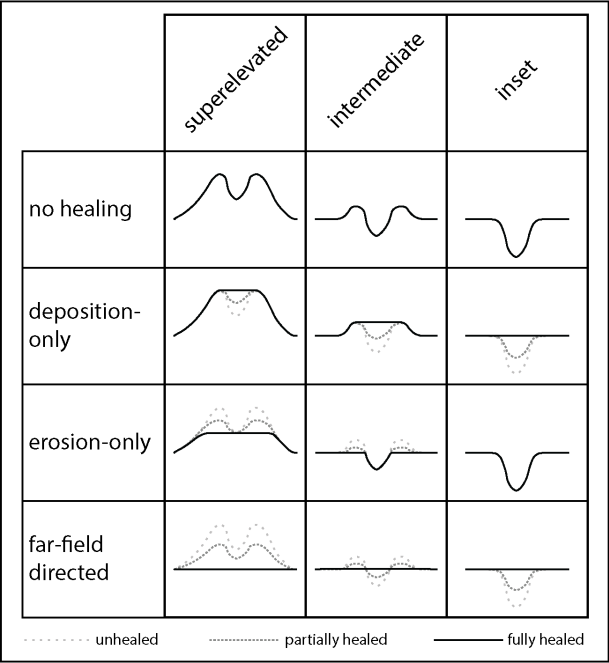
474 All healing modes adjust high, low, or both elevations linearly until a given endpoint is reached (Fig. 4). The healing
 475 rates are set to

$$476 \quad H_{high} = \alpha_{H,high} \frac{\bar{h}}{h_T} \quad (13a)$$

$$477 \quad H_{low} = \alpha_{H,low} \frac{\bar{h}}{h_T} \quad (13b)$$

478 where $\alpha_{H,high}$ and $\alpha_{H,low}$ are the healing rate parameters and have values that range from -1 to 1, and h_T is the characteristic
 479 time needed to heal one mean channel depth, which we set as 55,000 years (~~see Discussion for details on this value~~). ~~This~~
 480 ~~value~~ The value of h_T is necessarily speculative due to the lack of observational data on healing rates. ~~In light of these~~
 481 ~~uncertainties, we treated healing direction as an experimental parameter and assumed a healing timescale of 55 kyr. We came~~
 482 ~~to this~~our value by first estimating the fastest reasonable timescale over which an $O:10^0$ m deep abandoned channel (e.g.,
 483 oxbow lake) can be filled ~~based when on observed abandoned channel in filling rates ($O:10^{-2-3}$ m/yr) from ox-bow lakes it is~~
 484 ~~hydraulically connected to frequently flooding rivers (e.g. Cooper and McHenry 1989; Wren et al., 2008). This yields a~~
 485 ~~minimum h_T of $O:10^2-10^3$ yr. Abandoned channels must almost certainly heal slower than this rate, as most abandoned~~
 486 ~~channels are distant from the active channel at any given time (Figure 1, 2), and net sediment deposition rates are known to~~
 487 ~~decrease as observation window duration increases (Sadler 1981; Schumer and Jerolmack 2009). Next, we estimated~~We
 488 ~~established an upper limit to h_T as by estimating the equilibration timescale of an abandoned channel via diffusion alone,~~
 489 ~~which is on the order of $\frac{L^2}{\nu_{fp}}$ (Paola et al., 1992). For our case, L is a half-channel width (~50 meters) and ν_{fp} can be~~
 490 ~~approximated by hillslope diffusivity values (~0.005 square meters per year; Richardson et al., 2019). This yields a maximum~~
 491 ~~h_T of $O:10^5$ years. Thus~~Finally, we chose a representative h_T ~~between these two limit of 55,000 years. Future work is needed~~
 492 ~~to determine the validity of this assumed timescale, especially considering the importance of abandoned channels on affecting~~
 493 ~~avulsion set-up and pathfinding. Regardless, h_T is held constant between experimental runs, which instead vary only the~~
 494 ~~healing direction mode.~~ The first, ~~deposition-only~~ healing mode (deposition-only) raises abandoned channel lows toward
 495 levee-tops, such that $\alpha_{H,high} = 0$ and $\alpha_{H,low} = 1$. The second healing mode (erosion-only) lowers levees toward channel-
 496 bases, such that $\alpha_{H,high} = -1$ and $\alpha_{H,low} = 0$. The third healing mode (far-field directed) adjusts abandoned channel highs

497 and lows toward the far-field floodplain elevation at rates of $\alpha_{H,high} = -0.5$ and $\alpha_{H,low} = -0.5$. In all cases, once
498 topographic highs and lows have achieved their final healing endpoints (Fig. 4), $\alpha_{H,high}$ and $\alpha_{H,low}$ rates are set to 0.



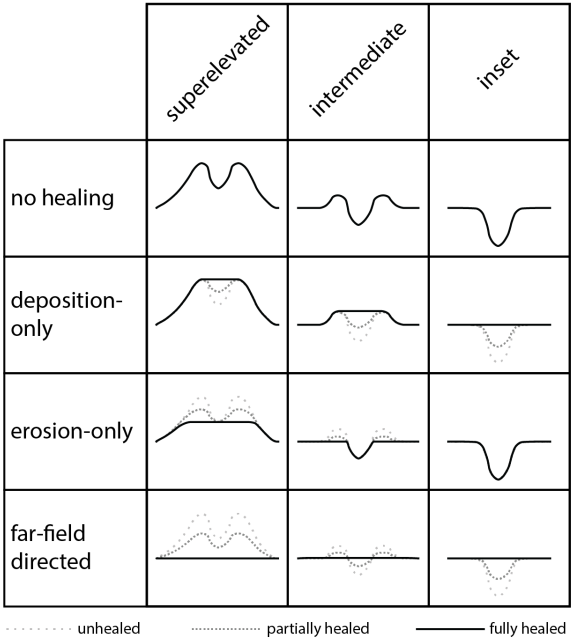


Figure 4: Potential healing modes for different initial conditions of abandoned channels. Each healing mode has different endpoints depending on the initial channel emplacement: deposition-only adjusts each abandoned channel cell’s low elevation toward its high elevation, erosion-only adjusts high elevations toward low elevations, and far-field directed adjusts both elevations towards the far-field floodplain elevation. As such, the deposition-only and erosion-only modes can result in topography that maintains positive topographic relief even once fully healed.

34.4. Experimental design

We ran four series of model experiments to investigate how abandoned channel attraction, repulsion, and healing influence avulsion dynamics. A summary of non-experimental and experimental parameters is provided in Table 3.

Table 3: Model parameters used to generate figures

Run duration (Myr)	Avulsion trigger period (years)	Healing timescale (h_T , years)	Initialization length (meters)	Repulsion factor (α_R)	Attraction factor (α_A)	Healing mode	Figure #
5	10	10,000	57,000	4.00	0.25	Far-field directed	5
1	30	55,000	122,500	4.00	0.25	Far-field directed	6,8,9
1	30	55,000	122,500	4.00	0.25	Far-field directed, deposition-only, and erosion-only	7
5	30	55,000	122,500	-0.50 to 8.00	0.25	Far-field directed	10
5	30	55,000	122,500	48.00	0.00 to 2.00	Far-field directed	11
10	30	55,000	122,500	4.00	0.25	Far-field directed, deposition-only, and erosion-only	12

The first series consists of a single base run with $\alpha_R = 4$, $\alpha_A = 0.25$, and far-field directed healing. Setting $\alpha_R = 4$ means that flow is repulsed when levees are four times the height of the approaching flow; this allows some channels to be repulsive and others to not. Setting $\alpha_A = 0.25$ allows channels to capture flow so long as they are deeper than $\frac{1}{4}$ of a mean channel depth, consistent with flume experiments (Reitz et al., 2010) that show old, in-filling abandoned channels acting as attractors with little remnant relief. For abandoned channel healing, we employed far-field directed healing because its endpoint of a totally flat plane is equivalent to that of diffusion on a laterally infinite plane, approximating the effects of floodplain diffusion without the computational cost.

Our second set of runs explored the importance of abandoned channel repulsion on where, when, and why avulsions occur by varying α_R from -0.50 (most repulsive) to 8 (least repulsive), while holding $\alpha_A = 0.25$. Each run is a 5 Myr simulation using the far-field directed healing mode.

Next, a matching third set of runs was performed to investigate the effect of α_A by varying it from 2.00 (least attractive) to 0 (most attractive) and setting $\alpha_R = 48$.

Our final set of runs investigated the role of abandoned channel healing mode without changing h_T (Fig. 4). We hold α_A and α_R constant over-between each 10 Myr run.

34.5 Analysis

We analyzed the planform appearance of generated topography and the location of avulsions for each run. For figures showing planform appearance (Fig. 5; Fig. 6; Fig. 10-12), we show each cell's high elevation normalized each-cell's high elevation relative to the $\eta_{farfield}$ for its row. We did this because megafans are low-relief features, and the change in elevation along dip otherwise overwhelms the signal (Fig. 5). We quantified avulsion locations by recording the straight-line distance from the mountain-front to each avulsion. These data were binned every 6.25 km and plotted as histograms showing the number of avulsions moving away from the upstream boundary. These values are normalized to the bin with the greatest occurrence.

For Fig. 6, we measured and binned avulsion locations in the same way for a second run without relative superelevation, but normalized this histogram to that of the base run to display the overall reduced number of avulsions. We also analysed avulsion locations by creating smoothed (50 kyr moving window average) curves of recorded distance to the mountain-front that show how median and 95th percentile (i.e., distal) avulsion locations change over the course of simulations. Finally, we analyzed differences between the proximal and distal domains for our base run by tracking the along-strike position of the active channel at two distances (12.5, 50 km) from the mountain-front for every timestep (Fig. 7).

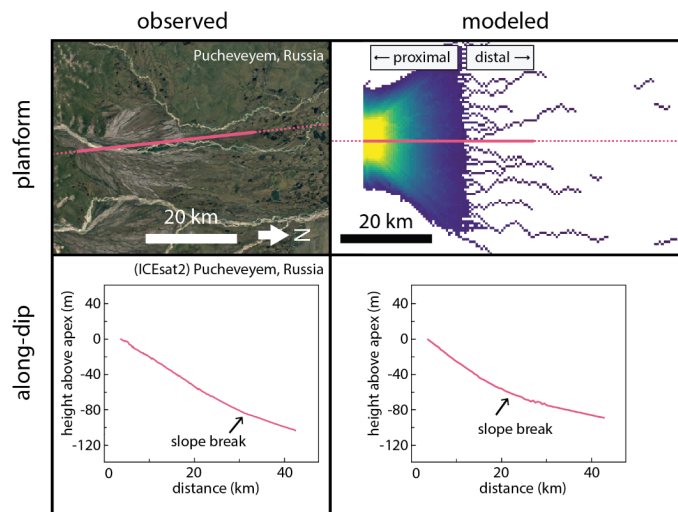
45. Model results

45.1. Base run and validation

We validated our model results by comparing model output for our base run with megafan topography from ICESat-2 (Neuenschwander et al., 2020) via the OpenAltimetry platform (Khalsa et al., 2020). ICESat-2 is a continuously measuring (10 kHz, ~0.7 m between points on the ground) satellite that collects vegetation-penetrating laser altimetry (Neuenschwander and Pitts, 2020). ICESat-2 offers greater precision than radar-derived elevation at the cost of limiting data collection to ~north-south oriented linear tracks. While our model does not aim to precisely simulate any specific fan, the simplified model recreates the essential features of mountain-front fluvial megafans. The 1D elevation diffusion model reproduces rivers with appropriate channel depths and slopes, while the 2D cellular model reproduces the change in broad, low-relief, cone- to fan-shaped topography typical of megafans along strike profiles of the Taquari megafan, showing broad, low-relief convex-up topographic profiles proximally that transition to nearly flat profiles in the distal domain (Fig. 5). Along-dip comparisons on the Pucheveyem fan (Fig. 5) are also favorable, showing similar low-relief slopes ($\sim 0.10^{-3}$). These slopes change abruptly at a topographic break marking the end of the fan topography, with a shallower gradient in the distal domain.

The model produces two distinct domains, consistent with earlier remote sensing observations (Fig. 1) despite no external parameters varying with distance to the mountain-front, aside from a linearly decreasing subsidence rate and increasing overbank aggradation rate. Further, these two domains still emerge within the model even when these two parameters are held uniform. The two domains generated are consistent with earlier remote sensing observations (Fig. 1). The proximal domain is a zone of sediment distribution created by repeated avulsions; it has a steeper slope (Fig. 5) and the abandoned channels that create the topography are radially distributive (Fig. 6A). In this domain, frequent channel avulsion causes small lateral adjustments to river position, filling local topographic lows (Fig. 7A). Avulsion probability is highest at the apex because that is where sediment is introduced (Fig. 6B). In contrast, the distal domain is a zone with a dominantly tributary geometry; it has a shallower slope (Fig. 5) and is much more sparsely channelized (Fig. 6A). In this domain, the active channel switches between fewer, more-persistent channels (Fig. 6A; Fig. 7A). Flow becomes confined to these more-persistent channels because avulsions that occur upstream are quickly captured and routed into one of a finite number of pre-existing pathways (Fig. 7A). Distal abandoned channels that are occupied infrequently can partially or fully heal between revisitations, creating discontinuous alluvial ridges (Fig. 2; Fig. 6). Avulsion probability rapidly decreases past the fan boundary (Fig. 6B).

565 ~~Past the fan boundary, and~~ along-strike topographic relief is nearly flat~~along-strike topographic profiles become nearly flat~~
566 ~~(Fig. 5), and which this~~ compares favorably to previous observations of megafans (Hartley et al., 2010a; Bernal et al., 2011).
567 ~~Notably, we reproduce these channel and megafan features despite the absence of bounding rivers or other external topographic~~
568 ~~controls that are seen on some modern megafans (Fig. 1E,F).~~



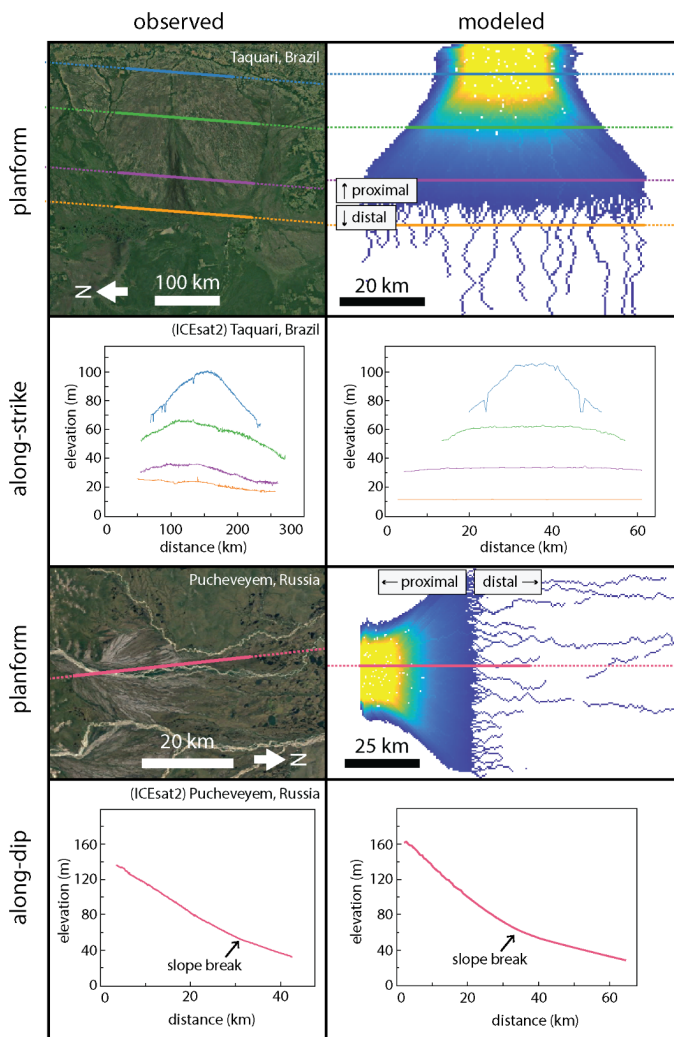
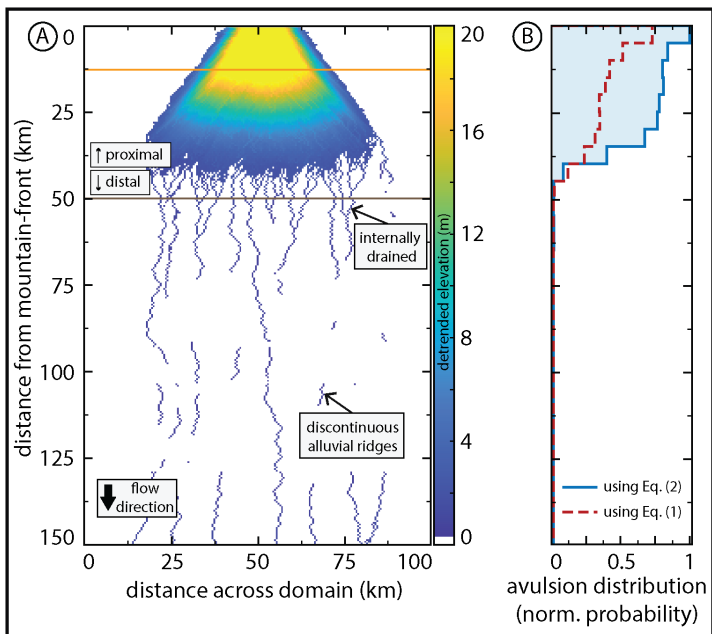


Figure 5: Megafan topography from model output compares favorably with real megafans observed in both the along-strike and along-dip profiles direction. Note the exceptional vertical exaggeration in the Taquari along-strike profiles, including delineation into distinct domains of slope. Colorbar and explanation for modelled planform is provided in Figure 6. Satellite images are USGS/NASA Landsat/Copernicus, © Google Earth.



575

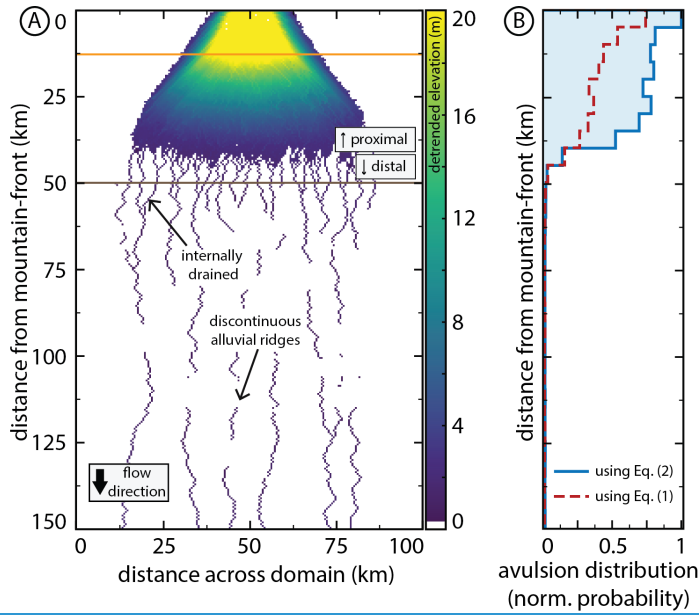
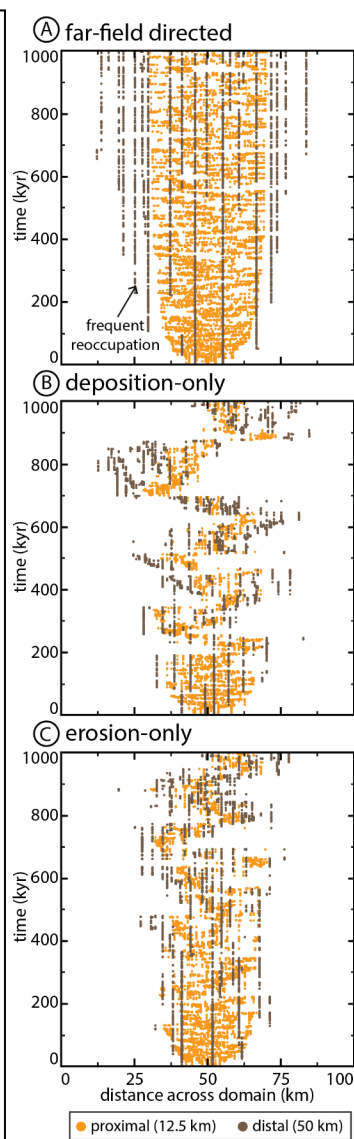
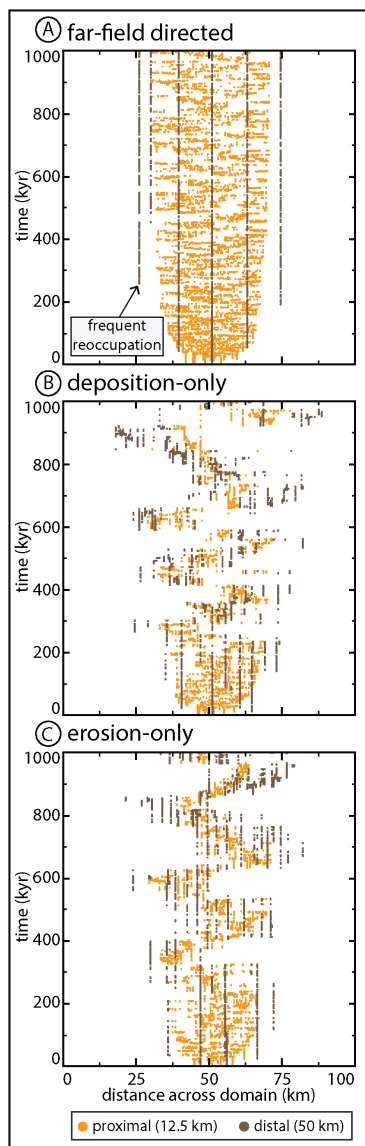


Figure 6: (a) Planform output of detrended high elevations from the base run. The colorbar is chosen such that negative or near-zero detrended values appear as white. The location of the active channel is not shown. The model produces two distinct domains (proximal and distal) in addition to several marked features which compare well with observed megafans in the real world (Fig. 1). Orange and dark brown horizontal lines show the proximal and distal measurement locations, respectively, for Fig. 7A. (b) A histogram (bin-width 6.25 km) showing the downstream distribution of avulsion loci. Blue line corresponds to output the model run shown in (A), whereas the dashed red line is the same as (a), but requires an equivalent run that differs by requiring one full channel depth of aggradation to achieve superelevation (Eq. (1)) instead of measuring elevation relative to adjacent cells (Eq. (2)). The run using Eq. (2) had a mean time between avulsions of 32 years, compared to 57 years for the run using Eq. (1). Vertical axis scale for (b) is the same as (a).



587 Figure 7: Active channel position histories over 1 Myr at two distances from the mountain-front for three runs. Distances to the
588 mountain-front are illustrated via horizontal bars in Fig. 6A and Fig. 12A. In each run, only one channel position is possible per
589 timestep. (a) A run using the same parameters as Fig. 6. Note frequent and continued reoccupation for distal river positions. (b) and
590 (c) show runs identical to (a) except the healing modes are deposition-only and erosion-only, respectively (Fig. 12A). These runs show
591 similar behavior to (a) in early years but transition to lobe-switching behavior. Distances to the mountain-front are illustrated via
592 horizontal bars in Fig. 6A.

593 4.2 How abandoned channels affect avulsion dynamics

594 Abandoned channels affect the timing and location of avulsions in four different ways: 1) superelevation shortcutting,
595 2) inheritance, 3) post-avulsion diffusion of the channel-bed, and 4) confluence aggradation. Each is discussed below.

596 We implemented avulsion set-up by measuring superelevation of an active channel relative to surrounding floodplain
597 topography (Eq. (2); Fig. 3). To investigate the effect of abandoned channels on this set-up, we performed an additional run
598 that is equivalent to our base run in Fig. 6 except for requiring each cell to aggrade a specified fraction ($\beta = 1$) of a channel
599 depth between each avulsion (Eq. (1); Fig. 6B). Compared to this run, the base run had a greater number of avulsions, especially
600 on the megafan surface downstream of the apex (Fig. 6B). Further, the run using Eq. (2) had a mean time between avulsions
601 of 32 years, compared to 57 years for the run using Eq. (1). Measuring superelevation relative to floodplains allows local
602 topographic lows associated with former abandoned channels to provide attractive locations for avulsion initiation, shortcutting
603 superelevation timescales (Jerolmack and Mohrig, 2007). Therefore, a densely channelized proximal domain generates
604 additional superelevation opportunities, spatially concentrating avulsions (Fig. 6B).

605 Abandoned channels also affect avulsion set-up indirectly through reoccupation mechanics. Superelevation is
606 inherited when avulsive flows reoccupy former abandoned channels. In a superelevated channel reach, an avulsion will strand
607 superelevated portions of the river that are downstream of the avulsion locus (discontinuous alluvial ridges in Fig. 6A). In this
608 way, avulsions can leave behind abandoned channels that may require minimal aggradation to achieve superelevation if they
609 are reoccupied before being healed, particularly if those channels are themselves adjacent to abandoned channel topography
610 that provides relative superelevation.

Formatted: Justified, Indent: First line: 0.5", Space After: 0 pt, Line spacing: 1.5 lines

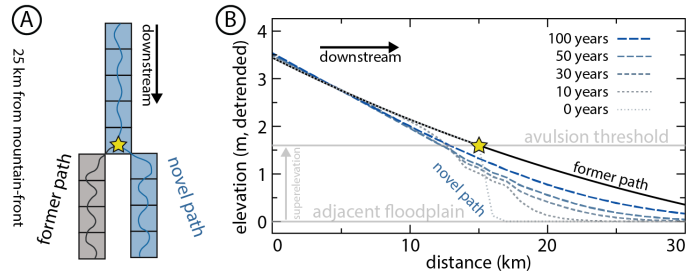
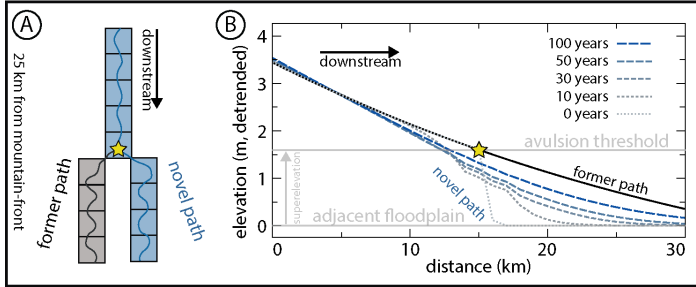


Figure 8: Model example showing channel evolution immediately after an avulsion, at a node marked by a star. (a) Planform arrangement of the parent channel and avulsion node, with both pathways of equal length. (b) Detrended elevation of the parent channel (relative to the adjacent floodplain) and new avulsion pathway upstream and downstream of the avulsion node. Immediately prior to the avulsion (black line), all cells upstream of the avulsion node are super-elevated and are equally likely to avulse if a trigger occurs. After the avulsion, gradual knickpoint propagation upstream reduces super-elevation. Downstream of the avulsion site, there is significant deposition that reduces the time to super-elevation.

In our model, avulsion set-up is also affected by local effects immediately after avulsions due to transient diffusion. This occurs in two ways. Firstly, super-elevated cells upstream of the avulsion locus are not instantly lowered but instead require time for the knickpoint to propagate upstream (Fig. 8). In our simulation, the post-avulsion upstream reduction in channel bed super-elevation proceeded gradually, migrating only several kilometers 100 years after an avulsion (Fig. 8). In this way, an avulsion does not instantly undo the avulsion set-up of cells upstream and future triggers can still cause avulsions to occur over this domain. Secondly, immediately downstream of an avulsion locus there is significant aggradation; a channel can diffuse nearly a meter of sediment into a downstream active channel cell within a decade (Fig. 8). In the case that these downstream cells are themselves already nearly super-elevated, this can provide sufficient aggradation above the adjacent floodplain to set-up these cells. This effect is even more pronounced when new active channel cells are adjacent to abandoned channel lows, and thus have lower super-elevation thresholds.

630 In our model, we observed abandoned channel confluences wherever a pathfinding flow is captured by a previous
631 abandoned channel. Captured channels follow steepest-descent pathfinding within the network of occupiable abandoned
632 channel cells. Within the distal, tributive domain, the number of possible abandoned channel pathways that can be occupied
633 decreases with increasing distance from the mountain-front (Fig. 6A; Fig. 7A). This allows locations downstream of
634 confluences to be more continuously occupied while the flow switches pathways upstream. This has important effects on
635 avulsion because more aggradation occurs downstream of the tributary junction. Consider a scenario where avulsions on the
636 fan always route flow into one of two possible paths (Fig. 9A,B). The pathway downstream of the confluence is occupied
637 100% of the time while each parent pathway is occupied approximately half of the time. As channel-bed aggradation occurs
638 only during active channel occupation, aggradation downstream of the confluence can therefore be greater than that observed
639 in either upstream pathway (Fig. 9C). As such, in the distal domain, abandoned channel reoccupation should preferentially
640 focus avulsions downstream of abandoned channel confluences.

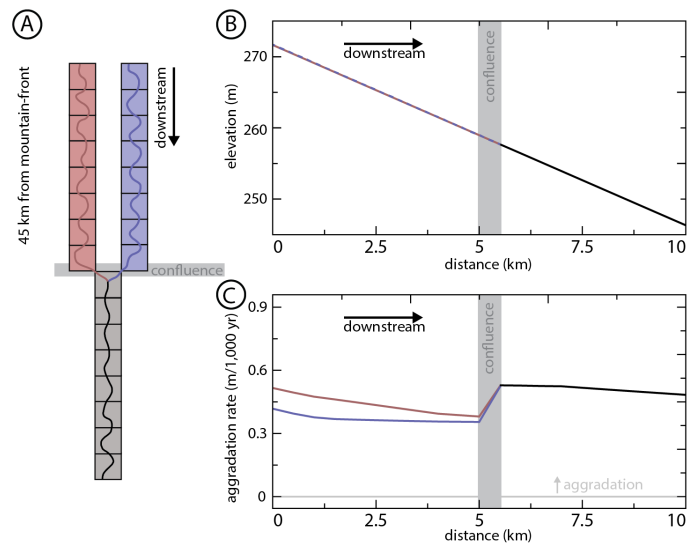
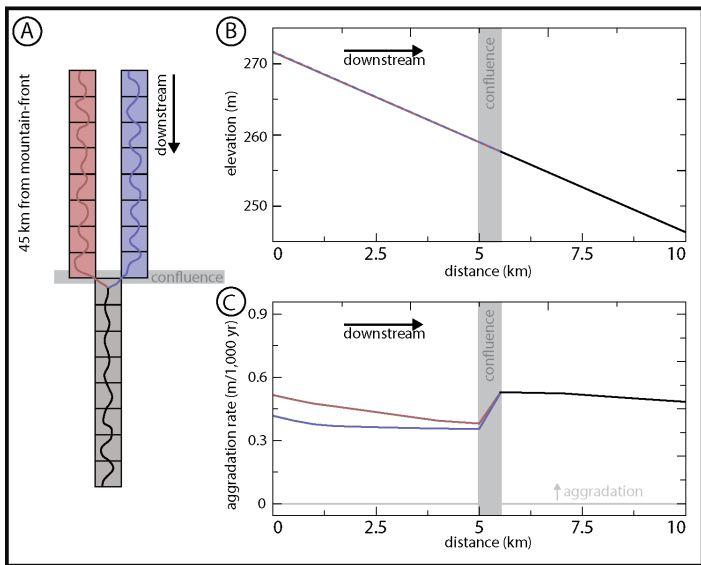


Figure 9: Model experiment showing channel evolution at an abandoned channel confluence. (a) Planform arrangement where the channel avulses between the red and blue pathways whenever normal avulsion criteria are satisfied. (b) Elevations of the red, blue, and gray channel segments upstream and downstream of the confluence. These elevations are not detrended. The blue channel profile is dashed to not obscure the red channel profile. (c) Aggradation rates over a 3,000 year period along the three channel segments. Repeated avulsions mean that the red and blue channels alternate deposition, while the gray channel downstream is constantly occupied leading to a faster aggradation downstream of the confluence.

4.3 Abandoned channel repulsion

We observed the effects of varying α_R on both planform appearance and the location of avulsions with a constant α_A (Fig. 10). Increasing repulsion (decreasing α_R) extends the proximal domain farther downstream; increasingly repulsive runs are increasingly distributive and generate fewer tributary confluences (Fig. 10A). Further, runs that are highly repulsive do not generate the abrupt downstream change in avulsion frequency seen when $\alpha_R \gg 21.00$. Instead, highly repulsive runs show relative avulsion frequencies that follow a power-law-like distribution with distance from the mountain-front (Fig. 10A).

The proximal domain propagates farther downstream when α_R is smaller (more repulsive) because avulsion location propagates farther downstream (Fig. 10B). While all avulsion location curves show a downstream progradation of avulsion locations during runs as the fan grows, both the median and 95th percentile shift downstream between runs with decreasing α_R when $\alpha_R \leq 1.00$ (i.e., where avulsive flows must be equal to or greater than levee heights above surrounding floodplains to reoccupy).

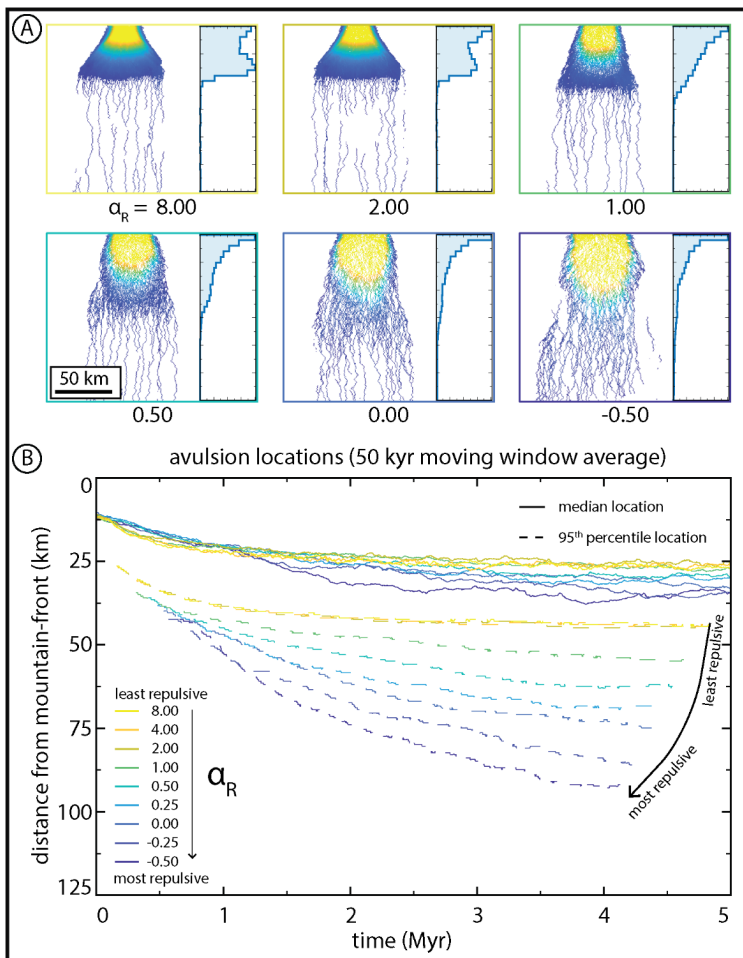
Median avulsion locations are less affected than 95th percentile curves, indicating that distribution skewness increases. The greatest shift in avulsion locations occurs between simulations employing $\alpha_R \leq 1.00$ (i.e., where avulsive flows must be equal to or greater than levee heights above surrounding floodplains to reoccupy).

Increasing repulsiveness (decreasing α_R) pushes avulsions farther from the mountain-front because flow in the proximal domain is concentrated into fewer channels, allowing for sediment (and therefore superelevation) to propagate farther downstream (Fig. 10). As a contributing effect, runs with lower α_R create more internally drained basins that themselves cause avulsions to fail. Since failed avulsions cause the timestep to increment without changing river positions, the time between successful avulsions is greater in runs with many failed avulsions, and sediment can thus propagate farther along active channels. This encourages channels in the distal part of the model to superelevate and avulse more often.

4.4 Abandoned channel attraction

Abandoned channel attraction dynamics also impact both avulsion locations and planform appearance during model runs (Fig. 11). With a constant α_R and increasing abandoned channel attraction (decreasing α_A), the transition from distributive to tributive domains shifts up-domain and fan width increases (Fig. 11A). When α_A is large (low attractiveness), model output resembles a series of weighted random walks because abandoned channels rarely capture flow and steepness weighted random walk determines channel position. Like the repulsion simulations, both the median and 95th percentile avulsion locations are affected by changing attraction parameters (Fig. 11B). Decreasing α_A (increasing attractiveness) pulls avulsions towards the mountain-front, and the greatest change is for α_A between ~0.50 and 1.50. Minimal change occurs for α_A values above and

677 below this range. In contrast, when α_A increases (attractiveness decreases), the fan lengthens and avulsions occur farther down-
678 domain because fan surfaces host abundant abandoned channels that influence avulsion dynamics. This interpretation is
679 supported by the avulsion histograms, where low-attractiveness runs show a non-zero avulsion frequency plateau in the distal
680 reaches and a more gradual downstream reduction in frequency than in more-attractive runs (Fig. 11A).



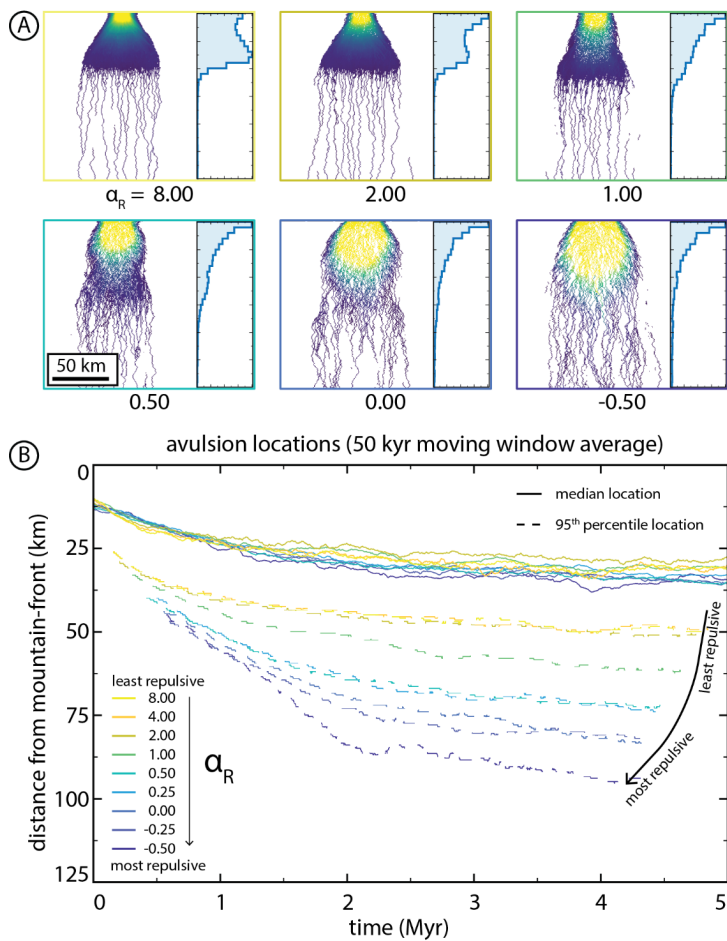
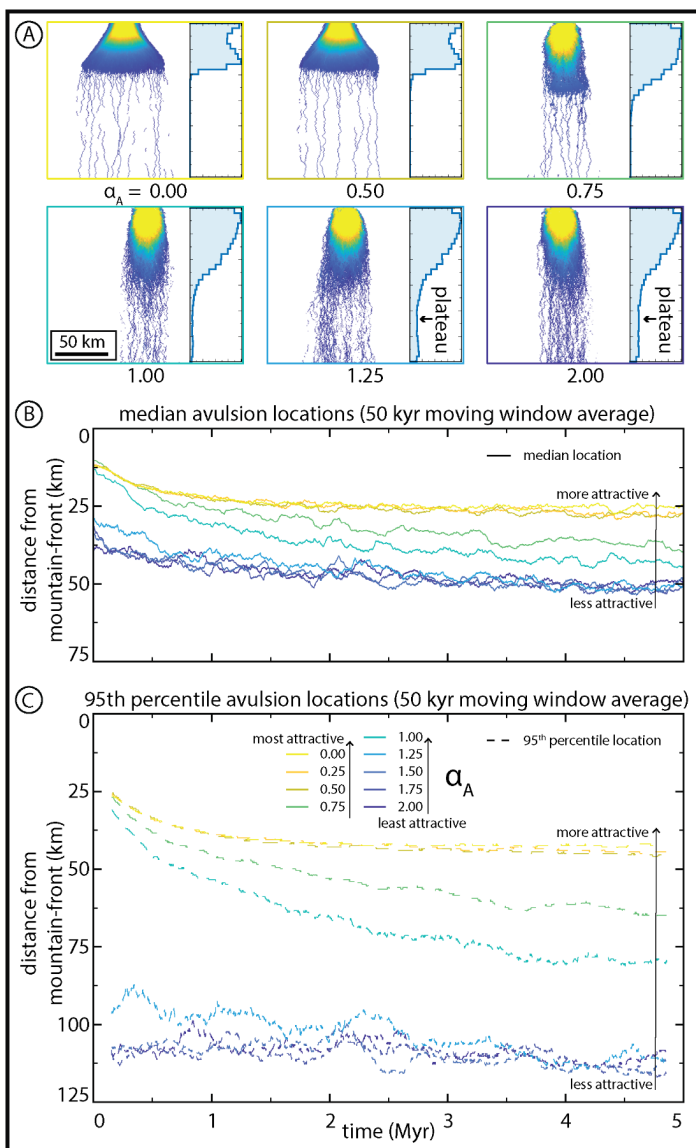


Figure 10: The effect of abandoned channel repulsion on (a) planform appearances and normalized avulsion location histograms, and (b) characteristic median avulsion locations through time. Decreasing α_R causes avulsion location to move downstream. These changes are more pronounced for 95th percentile locations. Color scale for inset planform appearances is the same as in Fig. 6.



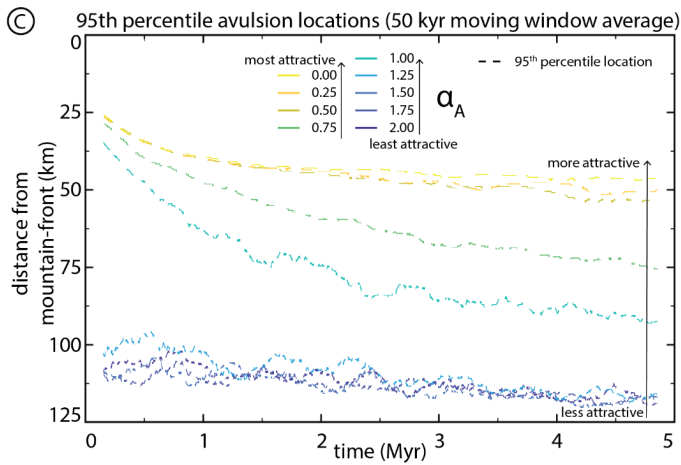
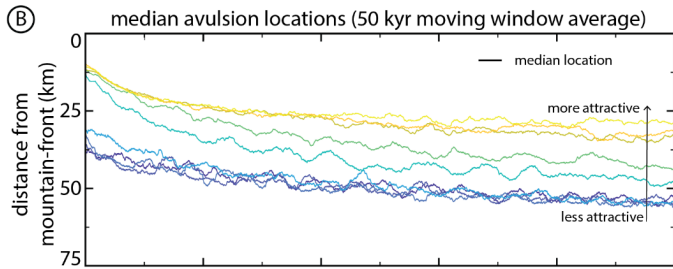
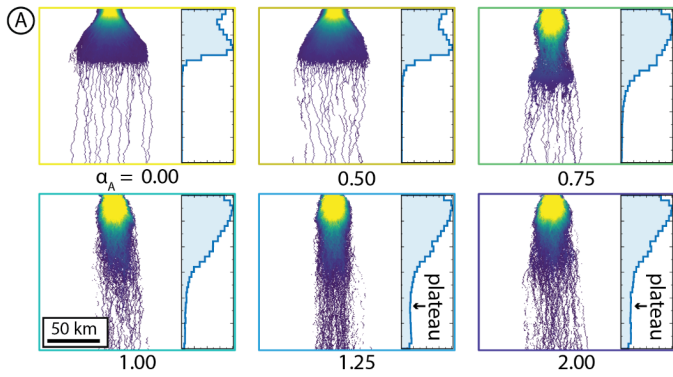


Figure 11: The effect of abandoned channel attraction on (a) planform appearances and normalized avulsion location histograms, and (b,c) characteristic avulsion locations through time. α_A legend and x-axis scale in (c) applies to (b) as well. Note the difference in y-axis ~~extents-range~~ between (b) and (c). Between α_A values of 0.50 and 1.50, increasing α_A causes predictable increases in the distance between the mountain-front and median and 95th percentile avulsion locations. These changes are more pronounced for 95th percentile locations, indicating greater skewness. Color scale for inset planform appearances is the same as in Fig. 6.

4.5.5 Healing mode

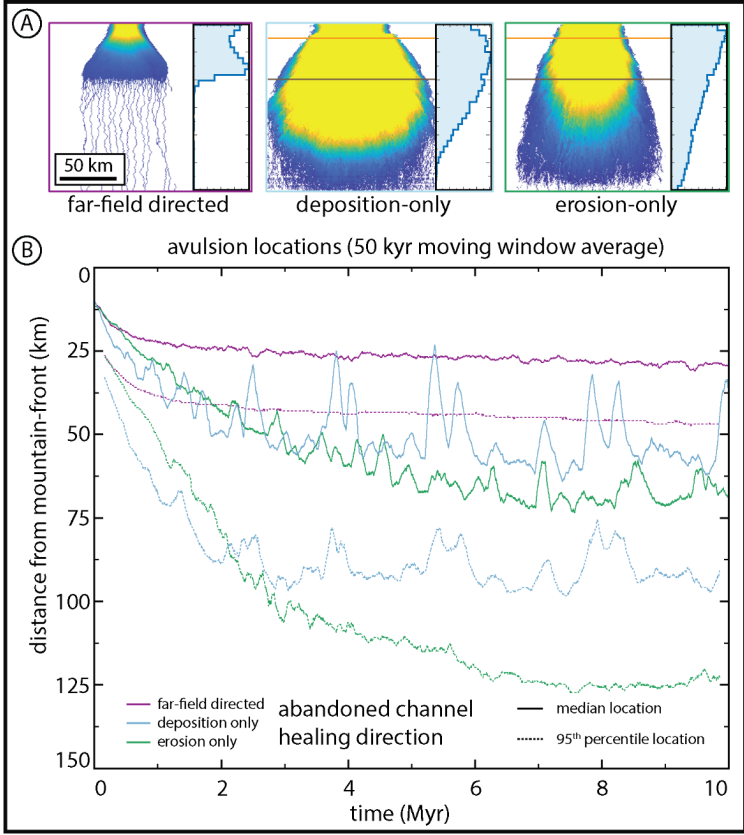
The healing mode determines how abandoned channels are gradually removed from the floodplain. By conducting 10 Myr base runs with different healing modes, we found that the deposition-only and erosion-only runs generated fans that nearly entirely filled up the simulation space over the course of several million years (Fig. 12). This occurs because the remnant topography of abandoned channels was never entirely removed by healing between visitations (Fig. 4). This is true even for the erosion-only run as, by definition, channels that achieve superelevation before abandonment have bases that are higher than surrounding floodplains. Since healing in erosion-only runs terminates once levees reach channel-beds, superelevated abandoned channel-beds on the floodplain remain indefinitely.

Healing mode affects avulsion location and introduces a new dynamic for fan growth. In erosion-only runs, the avulsion location ~~progrades-propagates~~ the farthest into the basin (Fig. 12B). Interestingly, the median and 95th percentile time series for deposition-only and erosion-only avulsion locations show spikes that represent avulsion location rapidly moving toward the mountain-front. These spikes represent lobe switching events, where avulsion loci shifted proximally as depositional space lower on the fan is filled and apical avulsions reroute flow to new regions on the fan surface (Fig. 7B,C; Supplemental Videos 1-3; DOI: 10.5446/54887). This compares well to observations of real-world megafans where deposition is interpreted to have occurred on discrete lobes (Chakraborty et al., 2010; Zani et al., 2012; Assine et al., 2014; Weissmann et al., 2015; Pupim et al., 2017). Lobe switching emerges in the model when deposition ~~is~~ is localized in a particular region ~~causes-asufficiently long for a~~ lobate area to become raised relative to other areas on the floodplain. This lowers the effective slope of this pathway, leading to a slope disadvantage over other regions on the floodplain. Future apical avulsions can then redirect flow to these other lower regions due to slope-weighted pathfinding, leading these lower regions to themselves eventually become raised and begin the cycle anew. Lobe switching does not occur during the earliest stages of fan growth because slopes are relatively steep on all faces of the fan and there is thus little intervening topography that could prevent an avulsing river from accessing other areas on the fan surface.

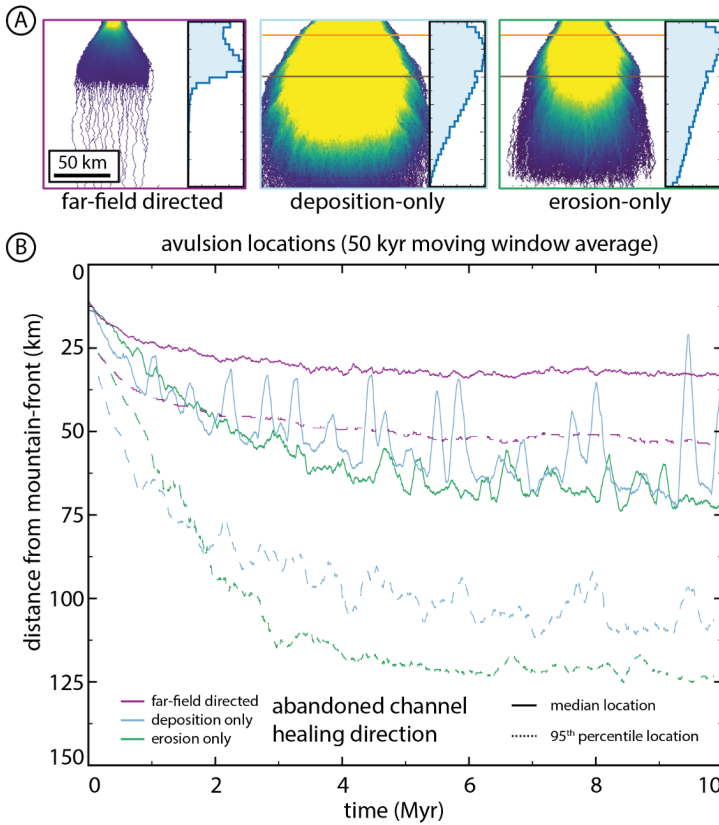
In contrast to the deposition-only and erosion-only runs, the far-field directed simulation achieved dynamic equilibrium relatively quickly and maintained a well-defined boundary between the proximal and distal domains for the remainder of the run. This occurs because it is the only healing mode that completely removes abandoned channel topography from floodplains. As such, this is the only healing mode that erases the topographic, attractive, and repulsive “memories” (*sensu* Reitz et al., 2010) of abandoned channels. Lobe switching on the same timescale is not observed in these runs because, unlike the deposition-only and erosion-only runs, far-field directed runs do not preserve topography indefinitely and alluvium is removed too quickly to build up regional slopes that can effectively resist pathfinding. Thus, while lobe switching seems to

722 have somewhat different frequencies based on whether abandoned channel healing is dominated by infilling or levee erosion,
723 the overall existence of lobe switching on this $O:10^5$ timescale is sensitive to the preservation potential of superelevated channel
724 beds and alluvial ridges.

725 It is important to note that both the erosion-only and deposition-only runs exhibited the typical separation of planform
726 space into two domains as they prograded, until the proximal domain encountered the edge of simulation space and the only
727 further adjustment that could occur was via vertical aggradation. Despite this, the deposition-only and erosion-only runs appear
728 to have less abrupt downstream avulsion frequency changes compared to the far-field directed one because the histograms are
729 time-integrated and reflect avulsion locations throughout the entire history of the run, including during progradation (Fig.
730 12A).



731



732

733 **Figure 12:** The effect of healing mode [on](#) (a) planform appearances and normalized avulsion location histograms, and (b)
 734 characteristic avulsion locations through time. Runs are identical other than employing different abandoned channel healing modes.
 735 Orange and dark brown horizontal lines show proximal and distal (respectively) distances from mountain-fronts for Fig. 7B
 736 (deposition-only) and 7C (erosion-only). Color scale for inset planform appearances is the same as in Fig. 6.

737 [56. Discussion](#)

738 [56.1 Model sensitivity to non-experimental parameters](#)

739 [Our model is generally insensitive to small variations within reasonable ranges for most parameters presented in](#)
 740 [Tables 1 and 2, including values for random walk weights, minimum superelevations \(\$\beta\$ \), overbank aggradation base rates](#)

Formatted: Normal

$A_{fp,base}$, subsidence rates (σ), initialization lengths, abandoned channel healing timescales (h_T), and incoming specific discharge and sediment supplies. One exception is that the overbank aggradation rate and subsidence rate at the bottom boundary of the domain must be equal to satisfy the downstream boundary condition, and if subsidence is much larger than aggradation upstream, the basin can sag due to underfilling over stratigraphic timescales. ~~Even when employing uniform subsidence,~~ We performed test runs with more functional changes, including runs that employed uniform subsidence (as opposed to foreland basin style subsidence), overbank deposition base values ($A_{fp,base}$) that did not change with distance to the mountain-front, or channel depths (h) and avulsion flow depths (h_{avul}) that did not vary along channel. In all cases, we still recreated the fundamental findings of two distinct emergent domains and the effects of abandoned channel repulsion, attraction, and healing on avulsion location.

56.1.2 Abandoned channels in avulsion models

Our model was designed to investigate the role of abandoned channels as both topographic repulsors and attractors during avulsion pathfinding. In doing so, we demonstrated effects on avulsion location and planform landscape evolution. We showed that abandoned channels affect the frequency and position of avulsions. Importantly, we demonstrated that the typical low-relief megafan with a transition from proximal (distributive, densely channelized) to distal (tributive, sparsely channelized) domains originates only when avulsion repulsion is infrequent and attraction is frequent (Fig. 10; Fig. 11). As such, when creating avulsion models, it is worth explicitly addressing abandoned channel creation, rate of healing, mode of healing, and interactions with future avulsion set-up and pathfinding because these factors fundamentally change avulsion dynamics and planform appearance of fluvial systems.

~~Abandoned channels and their impact on avulsion are usually ignored or grossly simplified in simulation models, especially in alluvial architecture models that simulate a 2D cross-section. The pioneering Leeder (1978), Allen (1978), and Bridge and Leeder (1979) models connected avulsions to alluvial architecture by creating 2D vertical slices of stratigraphy that result from channel avulsion across a basin over time. These models required heuristic rules about where successive rivers would be emplaced, including choosing locations randomly (Leeder, 1977), according to lowest elevation, (Bridge and Leeder, 1979), or randomly with abandoned channel repulsion (Allen, 1978). While their resulting stratigraphic sections were fairly insensitive to these differences (Hajek and Wolinsky, 2012), modern successors of these cross-section alluvial architecture models (e.g., Chamberlin and Hajek, 2015, 2019) have demonstrated that choosing different avulsion emplacement rules exerts a significant control on resulting stratigraphy. These rules position future channels along random (along a uniform distribution), compensational (at the lowest topographic elevation), or clustered (likelier to be nearer to the previous channel position) distributions. While these Previous stratigraphic models that simulate accumulation of channel bodies in a 2D strike-oriented cross-section have had to have employed rules in order to emplace prescribe the cross-basin location of successive channels without needing to resolveing planform pathfinding (Sect. 2), but the location and conditions that best fit each rule is not well known, it is unclear how abandoned channels affect or reflect each rule.~~

-. These rules typically are random, compensation (lowest elevation), or clustered (channel emplacement occurs near previous channel location). These rules create important differences in simulated alluvial stratigraphy (Chamberlain and Hajek, 2015), however Our results provide some mechanistic insight into the floodplain conditions that lead to different avulsion channel placement rules are unknown. An interesting outcome of our model Our results show is that the position of successive channels after avulsion follows different emplacement rules in proximal and distal domains for moderate attraction and repulsion (Fig. 7). In the proximal domain, avulsion pathways follow steepest-descent pathfinding that should generate compensational stratigraphy by seeking local, not global, topographic lows (Fig. 7). This correlates to a scheme where an avulsion is placed at the lowest elevation within a permissible lateral range (e.g., wide or narrow zone clustering of Chamberlin and Hajek, 2015), and This compares well to limited observational data showing that most avulsions initiate into topographic lows and travel relatively small lateral distances before joining abandoned channels (Edmonds et al., 2016; Valenza et al., 2020). In our deposition-only and erosion-only runs, emergent lobe switching provides an additional scale of clustering process that can control channel positions, creating both compensation (lobes switch to compensate) and clustering (channel switching within lobes) and compensation (lobes switch to compensate; (Fig. 7; Fig. 12). In the distal domain, channels are nearly perfectly clustered because however, flow routing instead switches between a small number of active channels in a network, each of which can heal if they are not revisited for a sufficient amount of time (Fig. 7). This compares better to the experimental model and flume observations of Jerolmack and Paola (2007) and Reitz et al. (2010). Finally, in the low attractiveness cases ($\alpha_A \geq 1$; Fig. 12), new channel pathways are determined entirely by slope-weighted random walk, which would compare closest to the compensational avulsion placement schemes of Chamberlin and Hajek (2015) or Bridge and Leeder (1979) or Chamberlin and Hajek (2015). As a caveat, when abandoned channels influence pathfinding, our model shows that it is not always possible for avulsions to find the globally lowest point in the whole domain for a given cross-section (cf. Bridge and Leeder, 1979) because there may be high topography in-between that prevents pathfinding. This is particularly evident in the lobe switching shown in Fig. 7B and Fig. 7C, where the global lowest point may exist outside of lobe deposition, but no viable route exists to reach that point.

To avoid making explicit assumptions about channel emplacement, a parallel lineage of avulsion models resolve avulsion dynamics and pathfinding in a planform basin. As such, these avulsion models require rules for hydrodynamics, sediment transport, and avulsion set-up, initiation, pathfinding, and stabilization, but allow for a more sophisticated interaction between avulsion pathfinding and floodplain topography (including abandoned channels) than can be resolved in cross-section models (Hajek and Wolinsky, 2012). Whenever these models incorporate steepness (with or without random noise) into avulsion pathfinding, and do not instantly erase the topographic alterations made by abandoned channels on landscapes, pathfinding is implicitly controlled by abandoned channels (e.g., Mackey and Bridge, 1995; Coulthard et al., 2002; Sun et al., 2002; Jerolmack and Paola, 2007; Reitz et al., 2010). As a broad classification, there are at least four assumptions that can describe the fate of these abandoned channels: i) avulsed channels do not leave behind abandoned channels on floodplains (instant healing; Ratliff et al., 2018, 2021), ii) abandoned channels do not change after avulsion (no healing), iii) abandoned channels are instantly healed after some fixed number of timesteps (Reitz et al., 2010), or iv) abandoned channels are healed

Formatted: Highlight

gradually over time by adjusting their channel base and/or levee top elevations (Jerolmack and Paola, 2007). The first three assumptions do not allow abandoned channel to act as both repulsors and attractors, which is inconsistent with observations of avulsing rivers (Edmonds et al., 2016; Valenza et al., 2020). Further, the first assumption generates no abandoned channel topography on floodplains, which is inconsistent with our observations (Fig. 2).

5.2.3 Floodplain topography and evolution

Our model shows that lobe switching on megafans only appears under certain abandoned channel healing rules (Fig. 7; Fig. 12). Floodplain topography, including abandoned channels, is thus a critical control on avulsion dynamics and landscape evolution and modelers who wish to recreate foreland basin topography must be conscious of how they choose to implement abandoned channel healing. While our results indicate that the preservation of abandoned channel topography between avulsions is necessary for lobe switching to emerge, further research can be directed towards uncovering other necessary conditions, and thus whether it is appropriate to assume that the presence of lobe switching on real world fans is a predictor of abandoned channel healing mode. This Regardless, the dependence of lobe switching on abandoned channel healing mode within our model result emphasizes Jerolmack and Paola (2007)'s identification of the remarkable lack of knowledge regarding the competing processes of topographic construction and destruction on floodplains. The principal topographic features of floodplains in aggradational (*sensu* Weissmann et al., 2015) settings appears to be abandoned channels, including both topographic highs and lows (Fig. 2). Understanding the extent to which abandoned channels and floodplain topography control avulsion dynamics in natural systems, requires a better understanding of floodplain topography. While little is known about the constructive and destructive processes in action on floodplains, we can speculate on the evolution of abandoned channels using observations from both degradational and aggradational settings (Hartley et al., 2010b).

There is field evidence that abandoned channels heal. During floods, overbank sediments can preferentially deposit in abandoned channel topographic lows (Wolman and Eiler, 1958; Schumde, 1963; Bridge and Leeder, 1979; Lewis and Lewin, 1983; Farrell, 1987; Nanson and Croke, 1992; Tooth et al., 2002; Jerolmack and Paola, 2007). This healing, however, can be undone in some cases by scouring from future flooding events (Wolman and Leopold, 1957; Wolman and Eiler, 1958; Schumde, 1963; Bridge and Leeder, 1979). What happens to abandoned channel highs, on the other hand, is not well understood. High elevation on floodplains could conceivably be eroded during subsequent flood events, or gradually diffused, similar to hillslopes (Roering et al., 1999). While floodplain slopes are characteristically low, biologic disturbance is high; it is not clear whether diffusion should also describe the evolution of alluvial floodplain topographic highs. Complicating matters, sediment deposition during overbank flows has also been observed atop flat or even positive floodplain topography, promoting self-sustaining topography that also hinders abandoned channel healing (Jahns, 1947; Wolman and Eiler, 1958; Schumde, 1963; Nanson, 1980).

Given the extent of these unknowns, considerable insight about floodplain evolution could be gained from highly detailed investigations of channel levees and beds before and after avulsions. Such investigations have been employed for abandoned channels in deltaic settings (e.g. Carlson et al., 2020), and similar work in fluvial settings could reveal the channel-

scale mechanics of abandoned channel attraction and repulsion in natural [fluvial systems](#) settings. Longitudinal studies of this nature could also understand the rate at which abandoned channels are healed (and thus no longer affect pathfinding) and the direction or mode in which they are healed, which we found to have important implications on avulsion dynamics (including lobe switching) and long-term planform morphology (Fig. 12). If abandoned channel healing rates are observed to vary spatially (for instance with distance [along-strike](#) from the active channel or [distance along-dip](#) from the mountain-front), this could motivate further modeling efforts. It may be that healing proceeds in different directions and at different rates in different settings in the basin, which will have important impacts on the spatial variation of avulsion dynamics and planform morphologies. We note that detailed work on the time-fate of topographic highs associated with abandoned channels is especially lacking in the body of literature. Finally, observations of avulsions in progress would help with understanding the appropriateness of our parameters α_R and α_A .

56.3.4 Next steps & predictions for comparison with field sites

We make several predictions that can motivate future observational and field studies. To begin, one key prediction is that in the proximal portions of foreland basins, avulsions should be most-frequent on the surfaces of megafans (e.g., Fig. 6B). These results compare favorably to the limited data available (Valenza et al., 2020) and can be tested by future observations of avulsions in the available and future remote sensing record. The emergence of future datasets on real-world avulsions should be able to confirm or deny the predicted abrupt, non-linear change in relative avulsion frequency with increasing distance from mountain-fronts on megafans (Fig. 6B). These data about the location of avulsions should also allow testing of other predictions from our model, including that avulsion in the distal domain of aggradational settings is more common immediately downstream of abandoned channel confluences due to a greater total occupancy duration and therefore greater total aggradation than either parent pathway immediately upstream (Fig. 8). [Finally, our model suggests that stratigraphic systems with evidence for clustering of channel avulsions \(e.g. the Ferris Formation; Hajek et al., 2010\) may have greater degrees of abandoned channel influence via attraction or lobe switching than systems that appear more randomly distributed \(e.g., the Williams Fork Formation; Chamberlin et al., 20176\).](#)

67. Conclusion

Abandoned channels are pervasive on megafans in modern foreland basin settings. These locations also have some of the highest avulsion rates in the observational record, [and thus necessitate which necessitates](#) considering the role of abandoned channels on avulsion dynamics and planform evolution in modeling efforts. We developed and presented a model that tests the interaction between abandoned channels and an avulsing river. Our model intrinsically generates two distinct domains, proximal and distal, in good comparison with remote sensing and previous research. We demonstrated that abandoned channels may shortcut avulsion superelevation timescales in these settings by providing topographic lows adjacent to potential avulsion loci, by providing remnant superelevation that can be inherited by future captured avulsions, including

871 downstream of abandoned channel confluences, and by transient knickpoint propagation that allows superelevated rivers to
872 remain superelevated upstream of the initial avulsion. The upshot of these factors is that avulsions are proportionately much
873 more common over the proximal distributive domain compared to the distal tributive one. We showed that tuning the degree
874 to which abandoned channel repulsion and attraction occur in simulations causes predictable changes in avulsion location
875 during those runs, whereby increasing repulsion pushes avulsions farther from the mountain-front, and increasing attraction
876 ‘pulls’ them closer. Next, we demonstrated the important role that abandoned channel healing mode has on gross planform
877 morphology, particularly over deep time, and that the proximal domain should grow until filling all available space in systems
878 that heal via deposition-only or erosion-only. Finally, we have highlighted opportunities for future work by field workers and
879 remote sensors in understanding the role that floodplain topography plays on avulsion dynamics, and the fate of floodplain
880 abandoned channel topography.

881 **78. Code Availability**

882 Our model code is written in MATLAB and is publicly and freely available (under the GPL v3 license) via GitHub
883 at the following DOI link: <https://doi.org/10.5281/zenodo.5576789>. The reference is included in our references list, under
884 harrison-martin, 2021. This can be updated as needed during the review process.

885 **89. Video supplement**

886 A video supplement (Supplemental Videos 1-3) is uploaded to the AV Portal of TIB Hannover under the CC BY-
887 NC-SA 3.0 DE license. The videos can be accessed at the following DOI links:
888 <https://doi.org/10.5446/54887> - Martin and Edmonds Avulsion Model Supplemental Video 1
889 <https://doi.org/10.5446/54888> - Martin and Edmonds Avulsion Model Supplemental Video 2
890 <https://doi.org/10.5446/54889> - Martin and Edmonds Avulsion Model Supplemental Video 3

891 **910. Author contribution**

892 HM and DE conceptualized and designed the research and developed the code. HM collected and analyzed the data,
893 wrote the manuscript, and prepared the figures. DE supervised the research and reviewed and edited the manuscript.

894 **1011. Competing interests**

895 The authors declare that they have no conflicts of interest.

896 **11.2. Acknowledgements**
 897 [HM was supported by NASA FINESST grant 80NSSC21K1598](#). HM and DE were supported by U.S. National
 898 Science Foundation grant EAR-1911321. We would like to thank Ben Peters for assistance with preparation of Figure 1. We
 899 would also like to thank Gary Weissmann and Jeffery Valenza for helpful conversations about rivers in foreland basins.

900 **12.13. Notation**

Symbol	Name	Units
A	non-dimensional constant	non-dimensional
A_{chan}	in-channel aggradation rate at some location	meters per year
$A_{fp,fbase}$	fixed-base rate component of overbank aggradation	meters per year
$A_{fp,tot}$	total overbank aggradation rate on the floodplain	meters per year
$A_{fp,v}$	variable rate component of overbank aggradation	meters per year
α_A	attraction factor	non-dimensional
$\alpha_{H,high}$	healing rate parameter for high elevations	non-dimensional
$\alpha_{H,low}$	healing rate parameter for low elevations	non-dimensional
α_R	repulsion factor	non-dimensional
β	channel depth fraction	non-dimensional
c_f	drag coefficient	non-dimensional
C_0	bed sediment concentration	non-dimensional
$\eta_{aban,high}$	abandoned channel levee elevation	meters
$\eta_{aban,low}$	abandoned channel bed elevation	meters
$\eta_{adj,low}$	channel bed elevation for a cell adjacent to the active channel	meters
$\eta_{appr,low}$	low elevation in the cell from which a pathfinding avulsion approaches an abandoned channel	meters
$\eta_{chan,high}$	levee elevation for an active channel cell	meters

$\eta_{chan,low}$	channel bed elevation for an active channel cell	meters
$\eta_{farfield}$	elevation of a far-field floodplain cell that has never been visited by the active channel	meters
$\eta_{fp,high}$	floodplain elevation, high	meters
$\eta_{fp,low}$	floodplain elevation, high	meters
$\eta_{high,max}$	the highest active, abandoned, or floodplain high elevation in a given row	meters
h_{aban}	remnant depth of an abandoned channel	meters
h_{avul}	flow depth of the pathfinding avulsion	meters
h_{chan}	active channel depth	meters
h_T	characteristic time needed to heal one mean channel depth	years
\bar{h}	mean flow depth	meters
H_{low}	healing rate for low elevations	meters per year
H_{high}	healing rate for high elevations	meters per year
L_h	levee height above approaching floodplain	meters per year
q	normalized water discharge per unit basin width	square meters per year
$\rho_{sediment}$	density of sediment	kilograms per cubic meter
ρ_{water}	density of water	kilograms per cubic meter
S	sediment specific gravity	non-dimensional
σ	subsidence rate	meters per year
t	time	years
T_A	Time time needed to achieve superelevation	years
ν	diffusivity	square meters per year
x	space	meters

1314. References

- Allen, J. R. L.: Studies in fluvial sedimentation: an exploratory quantitative model for the architecture of avulsion-controlled alluvial suites, *Sedimentary Geology*, 21, 129–147, [https://doi.org/10.1016/0037-0738\(78\)90002-7](https://doi.org/10.1016/0037-0738(78)90002-7), 1978.
- Aslan, A., Autin, W. J., and Blum, M. D.: Causes of River Avulsion: Insights from the Late Holocene Avulsion History of the Mississippi River, U.S.A., *Journal of Sedimentary Research*, 75, 650–664, <https://doi.org/10.2110/jsr.2005.053>, 2005.
- Assine, M. L.: River avulsions on the Taquari megafan, Pantanal wetland, Brazil, *Geomorphology*, 70, 357–371, <https://doi.org/10.1016/j.geomorph.2005.02.013>, 2005.
- Assine, M. L. and Soares, P. C.: Quaternary of the Pantanal, west-central Brazil, *Quaternary International*, 114, 23–34, [https://doi.org/10.1016/S1040-6182\(03\)00039-9](https://doi.org/10.1016/S1040-6182(03)00039-9), 2004.
- Assine, M. L., Corradini, F. A., Pupim, F. do N., and McGlue, M. M.: Channel arrangements and depositional styles in the São Lourenço fluvial megafan, Brazilian Pantanal wetland, *Sedimentary Geology*, 301, 172–184, <https://doi.org/10.1016/j.sedgeo.2013.11.007>, 2014.
- Bernal, C., Christophoul, F., Darrozes, J., Soula, J. C., Baby, P., and Burgos, J.: Late Glacial and Holocene avulsions of the Rio Pastaza Megafan (Ecuador-Peru): frequency and controlling factors, *Int J Earth Sci (Geol Rundsch)*, 100, 1759–1782, <https://doi.org/10.1007/s00531-010-0555-9>, 2011.
- Bokulich, A.: Explanatory Models Versus Predictive Models: Reduced Complexity Modeling in Geomorphology, in: *EPSA11 Perspectives and Foundational Problems in Philosophy of Science*, Cham, 115–128, https://doi.org/10.1007/978-3-319-01306-0_10, 2013.
- Bridge, J. S. and Leeder, M. R.: A simulation model of alluvial stratigraphy, 26, 617–644, <https://doi.org/10.1111/j.1365-3091.1979.tb00935.x>, 1979.
- Bryant, M., Falk, P., and Paola, C.: Experimental study of avulsion frequency and rate of deposition, *Geology*, 23, 365–368, [https://doi.org/10.1130/0091-7613\(1995\)023<0365:ESOFA>2.3.CO;2](https://doi.org/10.1130/0091-7613(1995)023<0365:ESOFA>2.3.CO;2), 1995.
- Buehler, H. A., Weissmann, G. S., Seuder, L. A., and Hartley, A. J.: Spatial and Temporal Evolution of an Avulsion on the Taquari River Distributive Fluvial System from Satellite Image Analysis, *Journal of Sedimentary Research*, 81, 630–640, <https://doi.org/10.2110/jsr.2011.040>, 2011.
- Burkham, D. E.: Channel Changes of the Gila River in Safford Valley, Arizona, 1846–1970, U.S. Government Printing Office, 36 pp., 1972.
- Chakraborty, T., Kar, R., Ghosh, P., and Basu, S.: Kosi megafan: Historical records, geomorphology and the recent avulsion of the Kosi River, *Quaternary International*, 227, 143–160, <https://doi.org/10.1016/j.quaint.2009.12.002>, 2010.
- Chamberlin, E. P. and Hajek, E. A.: Interpreting Paleo-Avulsion Dynamics from Multistory Sand Bodies, *Journal of Sedimentary Research*, 85, 82–94, <https://doi.org/10.2110/jsr.2015.09>, 2015.
- Chamberlin, E. P. and Hajek, E. A.: Using bar preservation to constrain reworking in channel-dominated fluvial stratigraphy, *Geology*, 47, 531–534, <https://doi.org/10.1130/G46046.1>, 2019.

934 Coulthard, T. J., Macklin, M. G., and Kirkby, M. J.: A cellular model of Holocene upland river basin and alluvial fan evolution,
935 27, 269–288, <https://doi.org/10.1002/esp.318>, 2002.

936 Croke, J., Fryirs, K., and Thompson, C.: Channel floodplain connectivity during an extreme flood event: implications for
937 sediment erosion, deposition, and delivery, 38, 1444–1456, <https://doi.org/10.1002/esp.3430>, 2013.

938 Edmonds, D. A., Hajek, E. A., Downton, N., and Bryk, A. B.: Avulsion flow-path selection on rivers in foreland basins,
939 *Geology*, 44, 695–698, <https://doi.org/10.1130/G38082.1>, 2016.

940 Edmonds, D. A., Martin, H. K., Valenza, J. M., Henson, R., Weissmann, G. S., Miltenberger, K., Mans, W., Moore, J. R.,
941 Slingerland, R. L., Gibling, M. R., Bryk, A. B., and Hajek, E. A.: Rivers in reverse: Upstream-migrating dechannelization and
942 flooding cause avulsions on fluvial fans, *Geology*, <https://doi.org/10.1130/G49318.1>, 2021.

943 Ethridge, F. G., Skelly, R. L., and Bristow, C. S.: Avulsion and Crevasing in the Sandy, Braided Niobrara River: Complex
944 Response to Base Level Rise and Aggradation, in: *Fluvial Sedimentology VI*, John Wiley & Sons, Ltd, 179–191,
945 <https://doi.org/10.1002/9781444304213.ch14>, 1999.

946 Farrell, K. M.: *Sedimentology and Facies Architecture of Overbank Deposits of the Mississippi River, False River Region,*
947 *Louisiana*, 1987.

948 Gabet, E. J.: Gopher bioturbation: field evidence for non-linear hillslope diffusion, 25, 1419–1428,
949 [https://doi.org/10.1002/1096-9837\(200012\)25:13<1419::AID-ESP148>3.0.CO;2-I](https://doi.org/10.1002/1096-9837(200012)25:13<1419::AID-ESP148>3.0.CO;2-I), 2000.

950 Gibling, M. R., Bashforth, A. R., Falcon-Lang, H. J., Allen, J. P., and Fielding, C. R.: Log Jams and Flood Sediment Buildup
951 Caused Channel Abandonment and Avulsion in the Pennsylvanian of Atlantic Canada, *Journal of Sedimentary Research*, 80,
952 268–287, <https://doi.org/10.2110/jsr.2010.024>, 2010.

953 Hack, J. T. and Goodlett, J. C.: *Geomorphology and forest ecology of a mountain region in the central Appalachians,*
954 *Geomorphology and forest ecology of a mountain region in the central Appalachians*, United States Government Printing
955 Office, Washington, D.C., <https://doi.org/10.3133/pp347>, 1960.

956 Hajek, E. A. and Wolinsky, M. A.: Simplified process modeling of river avulsion and alluvial architecture: Connecting models
957 and field data, *Sedimentary Geology*, 257–260, 1–30, <https://doi.org/10.1016/j.sedgeo.2011.09.005>, 2012.

958 harrison-martin: harrison-martin/RiverWalk: RiverWalk-AM-v1.0.0, <https://doi.org/10.5281/zenodo.5576789>, 18 October
959 2021.

960 Hartley, A. J., Weissmann, G. S., Nichols, G. J., and Seuderi, L. A.: Fluvial form in modern continental sedimentary basins:
961 Distributive fluvial systems: REPLY, *Geology*, 38, e231, <https://doi.org/10.1130/G31588Y.1>, 2010a.

962 Hartley, A. J., Weissmann, G. S., Nichols, G. J., and Warwick, G. L.: Large Distributive Fluvial Systems: Characteristics,
963 Distribution, and Controls on Development, *Journal of Sedimentary Research*, 80, 167–183,
964 <https://doi.org/10.2110/jsr.2010.016>, 2010b.

965 Harwood, K. and Brown, A. G.: Fluvial processes in a forested anastomosing river: Flood partitioning and changing flow
966 patterns, 18, 741–748, <https://doi.org/10.1002/esp.3290180808>, 1993.

967 Jahns, R. H.: Geologic features of the Connecticut Valley, Massachusetts, as related to recent floods,
968 <https://doi.org/10.3133/wsp996>, 1947.

969 Jerolmack, D. J.: Conceptual framework for assessing the response of delta channel networks to Holocene sea-level rise,
970 *Quaternary Science Reviews*, 28, 1786–1800, <https://doi.org/10.1016/j.quascirev.2009.02.015>, 2009.

971 Jerolmack, D. J. and Mohrig, D.: Conditions for branching in depositional rivers, *Geology*, 35, 463–466,
972 <https://doi.org/10.1130/G23308A.1>, 2007.

973 Jerolmack, D. J. and Paola, C.: Complexity in a cellular model of river avulsion, *Geomorphology*, 91, 259–270,
974 <https://doi.org/10.1016/j.geomorph.2007.04.022>, 2007.

975 Jones, L. S. and Schumm, S. A.: Causes of Avulsion: An Overview, in: *Fluvial Sedimentology VI*, John Wiley & Sons, Ltd,
976 169–178, <https://doi.org/10.1002/9781444304213.ch13>, 1999.

977 Khalsa, S. J. S., Borsari, A., Nandigam, V., Phan, M., Lin, K., Crosby, C., Fricker, H., Baru, C., and Lopez, L.: OpenAltimetry
978 –rapid analysis and visualization of Spaceborne altimeter data, *Earth Sci Inform*, [https://doi.org/10.1007/s12145-020-00520-](https://doi.org/10.1007/s12145-020-00520-2)
979 [2](https://doi.org/10.1007/s12145-020-00520-2), 2020.

980 Leeder, M. R.: A Quantitative Stratigraphic Model for Alluvium, with Special Reference to Channel Deposit Density and
981 Interconnectedness, 587–596, 1977.

982 Leier, A. L., DeCelles, P. G., and Pelletier, J. D.: Mountains, monsoons, and megafans, *Geology*, 33, 289–292,
983 <https://doi.org/10.1130/G21228.1>, 2005.

984 Lewis, G. W. and Lewin, J.: Alluvial Cutoffs in Wales and the Borderlands, in: *Modern and Ancient Fluvial Systems*, John
985 Wiley & Sons, Ltd, 145–154, <https://doi.org/10.1002/9781444303773.ch11>, 1983.

986 Mackey, S. D. and Bridge, J. S.: Three dimensional model of alluvial stratigraphy: theory and applications, *Journal of*
987 *Sedimentary Research*, 65, 7–31, <https://doi.org/10.1306/D42681D5-2B26-11D7-8648000102C1865D>, 1995.

988 Makaske, B., Maathuis, B. H. P., Padovani, C. R., Stölker, C., Mosselman, E., and Jongman, R. H. G.: Upstream and
989 downstream controls of recent avulsions on the Taquari megafan, Pantanal, south-western Brazil, 37, 1313–1326,
990 <https://doi.org/10.1002/esp.3278>, 2012.

991 Martin, Harrison K.; Edmonds, Douglas A.: Martin and Edmonds Avulsion Model Supplemental Video 1, Supplemental videos
992 of the paper "The push and pull of abandoned channels: How floodplain processes and healing affect avulsion dynamics and
993 alluvial landscape evolution in foreland basins". <https://doi.org/10.5446/54887>

994 Martin, Harrison K.; Edmonds, Douglas A.: Martin and Edmonds Avulsion Model Supplemental Video 2, Supplemental videos
995 of the paper "The push and pull of abandoned channels: How floodplain processes and healing affect avulsion dynamics and
996 alluvial landscape evolution in foreland basins". <https://doi.org/10.5446/54888>

997 Martin, Harrison K.; Edmonds, Douglas A.: Martin and Edmonds Avulsion Model Supplemental Video 3, Supplemental videos
998 of the paper "The push and pull of abandoned channels: How floodplain processes and healing affect avulsion dynamics and
999 alluvial landscape evolution in foreland basins". <https://doi.org/10.5446/54889>

1000 Martin, J., Sheets, B., Paola, C., and Hoyal, D.: Influence of steady base-level rise on channel mobility, shoreline migration,
1001 and sealing properties of a cohesive experimental delta, 114, <https://doi.org/10.1029/2008JF001142>, 2009.

1002 Mohrig, D., Heller, P. L., Paola, C., and Lyons, W. J.: Interpreting avulsion process from ancient alluvial sequences:
1003 Guadalupe-Matarranya system (northern Spain) and Wasatch Formation (western Colorado), GSA Bulletin, 112, 1787–1803,
1004 [https://doi.org/10.1130/0016-7606\(2000\)112<1787:IAPFAA>2.0.CO;2](https://doi.org/10.1130/0016-7606(2000)112<1787:IAPFAA>2.0.CO;2), 2000.

1005 Moodie, A. J., Nittrouer, J. A., Ma, H., Carlson, B. N., Chadwick, A. J., Lamb, M. P., and Parker, G.: Modeling Deltaic Lobe-
1006 Building Cycles and Channel Avulsions for the Yellow River Delta, China, 124, 2438–2462,
1007 <https://doi.org/10.1029/2019JF005220>, 2019.

1008 Morón, S., Amos, K., Edmonds, D. A., Payenberg, T., Sun, X., and Thyer, M.: Avulsion triggering by El Niño Southern
1009 Oscillation and tectonic forcing: The case of the tropical Magdalena River, Colombia, GSA Bulletin, 129, 1300–1313,
1010 <https://doi.org/10.1130/B31580.1>, 2017.

1011 Moudrý, V., Lecours, V., Gdulová, K., Gábor, L., Moudrá, L., Kropáček, J., and Wild, J.: On the use of global DEMs in
1012 ecological modelling and the accuracy of new bare-earth DEMs, Ecological Modelling, 383, 3–9,
1013 <https://doi.org/10.1016/j.ecolmodel.2018.05.006>, 2018.

1014 Nanson, G. C.: Point bar and floodplain formation of the meandering Beaton River, northeastern British Columbia, Canada,
1015 27, 3–29, <https://doi.org/10.1111/j.1365-3091.1980.tb01155.x>, 1980.

1016 Nanson, G. C. and Croke, J. C.: A genetic classification of floodplains, Geomorphology, 4, 459–486,
1017 [https://doi.org/10.1016/0169-555X\(92\)90039-Q](https://doi.org/10.1016/0169-555X(92)90039-Q), 1992.

1018 Neuenschwander, A. L. and Pitts, K.: Ice, Cloud, and Land Elevation Satellite 2 (ICESat-2) Algorithm Theoretical Basis
1019 Document (ATBD) for Land Vegetation Along Track Products (ATL08), [https://nsidc.org/sites/nsidc.org/files/technical-](https://nsidc.org/sites/nsidc.org/files/technical-references/ICESat2_ATL08_ATBD_r003.pdf)
1020 [references/ICESat2_ATL08_ATBD_r003.pdf](https://nsidc.org/sites/nsidc.org/files/technical-references/ICESat2_ATL08_ATBD_r003.pdf), 2020.

1021 Neuenschwander, A. L., Pitts, K., Jelley, B. P., Robbins, J., Klotz, B., Popescu, S. C., Nelson, R. F., Harding, D., Pederson,
1022 D., and Sheridan, R.: ATLAS/ICESat-2 L3A Land and Vegetation Height, version 3,
1023 <https://doi.org/10.5067/ATLAS/ATL08.003>, 2020.

1024 O'Loughlin, F. E., Paiva, R. C. D., Durand, M., Alsdorf, D. E., and Bates, P. D.: A multi-sensor approach towards a global
1025 vegetation corrected SRTM DEM product, Remote Sensing of Environment, 182, 49–59,
1026 <https://doi.org/10.1016/j.rse.2016.04.018>, 2016.

1027 Paola, C., Heller, P. L., and Angevine, C. L.: The large-scale dynamics of grain-size variation in alluvial basins, 1: Theory, 4,
1028 73–90, <https://doi.org/10.1111/j.1365-2117.1992.tb00145.x>, 1992.

1029 Pelletier, J. D., Mayer, L., Pearthree, P. A., House, P. K., Demsey, K. A., Klawon, J. E., and Vincent, K. R.: An integrated
1030 approach to flood hazard assessment on alluvial fans using numerical modeling, field mapping, and remote sensing, GSA
1031 Bulletin, 117, 1167–1180, <https://doi.org/10.1130/B25544.1>, 2005.

1032 Pizzuto, J. E.: Sediment diffusion during overbank flows, 34, 301–317, <https://doi.org/10.1111/j.1365-3091.1987.tb00779.x>,
1033 1987.

1034 Pupim, F. do N., Assine, M. L., and Sawakuchi, A. O.: Late Quaternary Cuiabá megafan, Brazilian Pantanal: Channel patterns
1035 and paleoenvironmental changes, *Quaternary International*, 438, 108–125, <https://doi.org/10.1016/j.quaint.2017.01.013>, 2017.

1036 Ratliff, K. M., Hutton, E. H. W., and Murray, A. B.: Exploring Wave and Sea-Level Rise Effects on Delta Morphodynamics
1037 With a Coupled River-Ocean Model, 123, 2887–2900, <https://doi.org/10.1029/2018JF004757>, 2018.

1038 Ratliff, K. M., Hutton, E. W. H., and Murray, A. B.: Modeling long-term delta dynamics reveals persistent geometric river
1039 avulsion locations, *Earth and Planetary Science Letters*, 559, 116786, <https://doi.org/10.1016/j.epsl.2021.116786>, 2021.

1040 Reitz, M. D., Jerolmack, D. J., and Swenson, J. B.: Flooding and flow-path selection on alluvial fans and deltas, 37,
1041 <https://doi.org/10.1029/2009GL041985>, 2010.

1042 Roering, J. J., Kirchner, J. W., and Dietrich, W. E.: Evidence for nonlinear, diffusive sediment transport on hillslopes and
1043 implications for landscape morphology, 35, 853–870, <https://doi.org/10.1029/1998WR900090>, 1999.

1044 Rossetti, D. F. and Valeriano, M. M.: Evolution of the lowest amazon basin modeled from the integration of geological and
1045 SRTM topographic data, *CATENA*, 70, 253–265, <https://doi.org/10.1016/j.catena.2006.08.009>, 2007.

1046 Schmudde, T. H.: Some Aspects of Land Forms of the Lower Missouri River Floodplain, 53, 60–73, 1963.

1047 Slingerland, R. and Kump, L.: *Mathematical Modeling of Earth's Dynamical Systems: A Primer*, Princeton University Press,
1048 246 pp., 2011.

1049 Slingerland, R. and Smith, N.: River avulsions and deposits, *Annual Review of Earth and Planetary Sciences*, 32, 257–285,
1050 <https://doi.org/10.1146/annurev.earth.32.101802.120201>, 2004.

1051 Smith, N., Slingerland, R., Pérez-Arlucea, M., and Morozova, G.: The 1870s avulsion of the Saskatchewan River, *Canadian*
1052 *Journal of Earth Sciences*, 35, 453–466, <https://doi.org/10.1139/cjes-35-4-453>, 1998.

1053 Sun, T., Paola, C., Parker, G., and Meakin, P.: Fluvial fan deltas: Linking channel processes with large-scale morphodynamics,
1054 38, 26–1–26–10, <https://doi.org/10.1029/2001WR000284>, 2002.

1055 Toonen, W. H. J., Kleinhans, M. G., and Cohen, K. M.: Sedimentary architecture of abandoned channel fills, 37, 459–472,
1056 <https://doi.org/10.1002/esp.3189>, 2012.

1057 Tooth, S., McCarthy, T. S., Brandt, D., Hancox, P. J., and Morris, R.: Geological controls on the formation of alluvial meanders
1058 and floodplain wetlands: the example of the Klip River, eastern Free State, South Africa, 27, 797–815,
1059 <https://doi.org/10.1002/esp.353>, 2002.

1060 Valenza, J. M., Edmonds, D. A., Hwang, T., and Roy, S.: Downstream changes in river avulsion style are related to channel
1061 morphology, 11, 2116, <https://doi.org/10.1038/s41467-020-15859-9>, 2020.

1062 Weissmann, G., Hartley, A., Seuderi, L., Nichols, G., Davidson, S., Owen, A., Atchley, S., Bhattacharyya, P., Chakraborty,
1063 T., Ghosh, A., Nordt, L., Michel, L., and Tabor, N.: Prograding distributive fluvial systems: Geomorphic models and ancient
1064 examples, <https://doi.org/10.2110/sepm.104.16>, 1 January 2013.

1065 Weissmann, G. S., Hartley, A. J., Nichols, G. J., Seuderi, L. A., Olson, M., Buehler, H., and Banteah, R.: Fluvial form in
1066 modern continental sedimentary basins: Distributive fluvial systems, *Geology*, 38, 39–42, <https://doi.org/10.1130/G30242.1>,
1067 2010.

1068 [Weissmann, G. S., Hartley, A. J., Seuderi, L. A., Nichols, G. J., Owen, A., Wright, S., Felicia, A. L., Holland, F., and Anaya,](#)
1069 [F. M. L.: Fluvial geomorphic elements in modern sedimentary basins and their potential preservation in the rock record: A](#)
1070 [review, *Geomorphology*, 250, 187–219, <https://doi.org/10.1016/j.geomorph.2015.09.005>, 2015.](#)

1071 [Wells, N. A. and Dorr, J. A.: A Reconnaissance of Sedimentation on the Kosi Alluvial Fan of India, 14, 1987.](#)

1072 [Wolman, M. G. and Eiler, J. P.: Reconnaissance study of erosion and deposition produced by the flood of August 1955 in](#)
1073 [Connecticut, 39, 1–14, <https://doi.org/10.1029/TR039i001p00001>, 1958.](#)

1074 [Wolman, M. G. and Leopold, L. B.: River flood plains: Some observations on their formation, *River flood plains: Some*
1075 \[observations on their formation, U.S. Government Printing Office, Washington, D.C., <https://doi.org/10.3133/pp282C>, 1957.\]\(#\)](#)

1076 [Zani, H., Assine, M. L., and McGlue, M. M.: Remote sensing analysis of depositional landforms in alluvial settings: Method](#)
1077 [development and application to the Taquari megafan, Pantanal \(Brazil\), *Geomorphology*, 161–162, 82–92,](#)
1078 [https://doi.org/10.1016/j.geomorph.2012.04.003, 2012.](#)

1079 [Zwoliński, Z.: Sedimentology and geomorphology of overbank flows on meandering river floodplains, *Geomorphology*, 4,](#)
1080 [367–379, \[https://doi.org/10.1016/0169-555X\\(92\\)90032-J\]\(https://doi.org/10.1016/0169-555X\(92\)90032-J\), 1992.](#)

1081

1082

1083 [Allen, J. R. L.: Studies in fluvial sedimentation: an exploratory quantitative model for the architecture of avulsion-controlled](#)
1084 [alluvial suites, *Sedimentary Geology*, 21, 129–147, \[https://doi.org/10.1016/0037-0738\\(78\\)90002-7\]\(https://doi.org/10.1016/0037-0738\(78\)90002-7\), 1978.](#)

1085 [Aslan, A., Autin, W. J., and Blum, M. D.: Causes of River Avulsion: Insights from the Late Holocene Avulsion History of the](#)
1086 [Mississippi River, U.S.A., *Journal of Sedimentary Research*, 75, 650–664, <https://doi.org/10.2110/jsr.2005.053>, 2005.](#)

1087 [Assine, M. L.: River avulsions on the Taquari megafan, Pantanal wetland, Brazil, *Geomorphology*, 70, 357–371,](#)
1088 [https://doi.org/10.1016/j.geomorph.2005.02.013, 2005.](#)

1089 [Assine, M. L. and Soares, P. C.: Quaternary of the Pantanal, west-central Brazil, *Quaternary International*, 114, 23–34,](#)
1090 [https://doi.org/10.1016/S1040-6182\(03\)00039-9, 2004.](#)

1091 [Assine, M. L., Corradini, F. A., Pupim, F. do N., and McGlue, M. M.: Channel arrangements and depositional styles in the](#)
1092 [São Lourenço fluvial megafan, Brazilian Pantanal wetland, *Sedimentary Geology*, 301, 172–184,](#)
1093 [https://doi.org/10.1016/j.sedgeo.2013.11.007, 2014.](#)

1094 [Bernal, C., Christophoul, F., Darrozes, J., Soula, J.-C., Baby, P., and Burgos, J.: Late Glacial and Holocene avulsions of the](#)
1095 [Rio Pastaza Megafan \(Ecuador–Peru\): frequency and controlling factors, *Int J Earth Sci \(Geol Rundsch\)*, 100, 1759–1782,](#)
1096 [https://doi.org/10.1007/s00531-010-0555-9, 2011.](#)

1097 [Bokulich, A.: Explanatory Models Versus Predictive Models: Reduced Complexity Modeling in Geomorphology, in: *EPSA11*](#)
1098 [Perspectives and Foundational Problems in Philosophy of Science, Cham, 115–128, \[https://doi.org/10.1007/978-3-319-01306-\]\(https://doi.org/10.1007/978-3-319-01306-0_10\)](#)
1099 [0_10, 2013.](#)

1100 [Bridge, J. S. and Leeder, M. R.: A simulation model of alluvial stratigraphy, 26, 617–644, \[3091.1979.tb00935.x, 1979.\]\(https://doi.org/10.1111/j.1365-

1101 <a href=\)](#)

1102 Bryant, M., Falk, P., and Paola, C.: Experimental study of avulsion frequency and rate of deposition, *Geology*, 23, 365–368,
1103 [https://doi.org/10.1130/0091-7613\(1995\)023<0365:ESOFA>2.3.CO;2](https://doi.org/10.1130/0091-7613(1995)023<0365:ESOFA>2.3.CO;2), 1995.

1104 Buehler, H. A., Weissmann, G. S., Scuderi, L. A., and Hartley, A. J.: Spatial and Temporal Evolution of an Avulsion on the
1105 Taquari River Distributive Fluvial System from Satellite Image Analysis, *Journal of Sedimentary Research*, 81, 630–640,
1106 <https://doi.org/10.2110/jsr.2011.040>, 2011.

1107 Burkham, D. E.: *Channel Changes of the Gila River in Safford Valley, Arizona, 1846-1970*, U.S. Government Printing Office,
1108 36 pp., 1972.

1109 Carlson, B. N., Nitttrouer, J. A., Moodie, A. J., Kineke, G. C., Kumpf, L. L., Ma, H., Parsons, D. R., and Wang, H.: Infilling
1110 Abandoned Deltaic Distributary Channels Through Landward Sediment Transport, *Journal of Geophysical Research: Earth*
1111 *Surface*, 125, e2019JF005254, <https://doi.org/10.1029/2019JF005254>.

1112 Chakraborty, T., Kar, R., Ghosh, P., and Basu, S.: Kosi megafan: Historical records, geomorphology and the recent avulsion
1113 of the Kosi River, *Quaternary International*, 227, 143–160, <https://doi.org/10.1016/j.quaint.2009.12.002>, 2010.

1114 Chamberlin, E. P., Hajek, E. A., and Trampus, S. M.: Measuring Scales of Autogenic Organization in Fluvial Stratigraphy:
1115 An Example from the Cretaceous Lower Williams Fork Formation, Colorado, in: *Autogenic Dynamics and Self-Organization*
1116 *in Sedimentary Systems*, SEPM Society for Sedimentary Geology, 106, 132-144, [http://dx.doi.org/10.2110/sepm.106.07.](http://dx.doi.org/10.2110/sepm.106.07.2016),
1117 2016.

1118 Chamberlin, E. P. and Hajek, E. A.: Interpreting Paleo-Avulsion Dynamics from Multistory Sand Bodies, *Journal of*
1119 *Sedimentary Research*, 85, 82–94, <https://doi.org/10.2110/jsr.2015.09>, 2015.

1120 Chamberlin, E. P. and Hajek, E. A.: Using bar preservation to constrain reworking in channel-dominated fluvial stratigraphy,
1121 *Geology*, 47, 531–534, <https://doi.org/10.1130/G46046.1>, 2019.

1122 Cooper, C. M. and Henry, J. R.: Sediment accumulation and its effects on a Mississippi River oxbow lake, *Environmental*
1123 *Geology and Water Sciences*, 13, 33-37, <https://doi.org/10.1007/BF01666569>, 1989.

1124 Coulthard, T. J., Macklin, M. G., and Kirkby, M. J.: A cellular model of Holocene upland river basin and alluvial fan evolution,
1125 *27*, 269–288, <https://doi.org/10.1002/esp.318>, 2002.

1126 Croke, J., Fryirs, K., and Thompson, C.: Channel–floodplain connectivity during an extreme flood event: implications for
1127 sediment erosion, deposition, and delivery, *38*, 1444–1456, <https://doi.org/10.1002/esp.3430>, 2013.

1128 Edmonds, D. A., Hajek, E. A., Downton, N., and Bryk, A. B.: Avulsion flow-path selection on rivers in foreland basins,
1129 *Geology*, 44, 695–698, <https://doi.org/10.1130/G38082.1>, 2016.

1130 Edmonds, D. A., Martin, H. K., Valenza, J. M., Henson, R., Weissmann, G. S., Miltenberger, K., Mans, W., Moore, J. R.,
1131 Slingerland, R. L., Gibling, M. R., Bryk, A. B., and Hajek, E. A.: Rivers in reverse: Upstream-migrating dechannelization and
1132 flooding cause avulsions on fluvial fans, *Geology*, 50, 37–41, <https://doi.org/10.1130/G49318.1>, 2022.

1133 Ethridge, F. G., Skelly, R. L., and Bristow, C. S.: Avulsion and Crevasse in the Sandy, Braided Niobrara River: Complex
1134 Response to Base-Level Rise and Aggradation, in: *Fluvial Sedimentology VI*, John Wiley & Sons, Ltd, 179–191,
1135 <https://doi.org/10.1002/9781444304213.ch14>, 1999.

Formatted: Default Paragraph Font

Formatted: Default Paragraph Font

136 [Farrell, K. M.: Sedimentology and Facies Architecture of Overbank Deposits of the Mississippi River, False River Region,](#)
137 [Louisiana, 1987.](#)

138 [Gabet, E. J.: Gopher bioturbation: field evidence for non-linear hillslope diffusion, 25, 1419–1428,](#)
139 [Gibling, M. R., Bashforth, A. R., Falcon-Lang, H. J., Allen, J. P., and Fielding, C. R.: Log Jams and Flood Sediment Buildup](https://doi.org/10.1002/1096-9837(200012)25:13<1419::AID-ESP148>3.0.CO;2-1, 2000.</p>
<p>140 <a href=)
141 [Caused Channel Abandonment and Avulsion in the Pennsylvanian of Atlantic Canada, Journal of Sedimentary Research, 80,](#)
142 [268–287, <https://doi.org/10.2110/jsr.2010.024>, 2010.](#)

143 [Hack, J. T. and Goodlett, J. C.: Geomorphology and forest ecology of a mountain region in the central Appalachians,](#)
144 [Geomorphology and forest ecology of a mountain region in the central Appalachians, United States Government Printing](#)
145 [Office, Washington, D.C., <https://doi.org/10.3133/pp347>, 1960.](#)

146 [Hajek, E. A. and Wolinsky, M. A.: Simplified process modeling of river avulsion and alluvial architecture: Connecting models](#)
147 [and field data, Sedimentary Geology, 257–260, 1–30, <https://doi.org/10.1016/j.sedgeo.2011.09.005>, 2012.](#)

148 [Hajek, E. A., Heller, P. L., and Sheets, B. A.: Significance of channel-belt clustering in alluvial basins, Geology, 38, 535–538,](#)
149 [<https://doi.org/10.1130/G30783.1>, 2010.](#)

150 [harrison-martin: harrison-martin/RiverWalk: RiverWalk-AM v1.0.0, <https://doi.org/10.5281/zenodo.5576789>, 18 October](#)
151 [2021.](#)

152 [Hartley, A. J., Weissmann, G. S., Nichols, G. J., and Scuderi, L. A.: Fluvial form in modern continental sedimentary basins:](#)
153 [Distributive fluvial systems: REPLY, Geology, 38, e231, <https://doi.org/10.1130/G31588Y.1>, 2010a.](#)

154 [Hartley, A. J., Weissmann, G. S., Nichols, G. J., and Warwick, G. L.: Large Distributive Fluvial Systems: Characteristics,](#)
155 [Distribution, and Controls on Development, Journal of Sedimentary Research, 80, 167–183,](#)
156 [<https://doi.org/10.2110/jsr.2010.016>, 2010b.](#)

157 [Harwood, K. and Brown, A. G.: Fluvial processes in a forested anastomosing river: Flood partitioning and changing flow](#)
158 [patterns, 18, 741–748, <https://doi.org/10.1002/esp.3290180808>, 1993.](#)

159 [Jahns, R. H.: Geologic features of the Connecticut Valley, Massachusetts, as related to recent floods,](#)
160 [<https://doi.org/10.3133/wsp996>, 1947.](#)

161 [Jerolmack, D. J.: Conceptual framework for assessing the response of delta channel networks to Holocene sea level rise,](#)
162 [Quaternary Science Reviews, 28, 1786–1800, <https://doi.org/10.1016/j.quascirev.2009.02.015>, 2009.](#)

163 [Jerolmack, D. J. and Mohrig, D.: Conditions for branching in depositional rivers, Geology, 35, 463–466,](#)
164 [<https://doi.org/10.1130/G23308A.1>, 2007.](#)

165 [Jerolmack, D. J. and Paola, C.: Complexity in a cellular model of river avulsion, Geomorphology, 91, 259–270,](#)
166 [<https://doi.org/10.1016/j.geomorph.2007.04.022>, 2007.](#)

167 [Jones, L. S. and Schumm, S. A.: Causes of Avulsion: An Overview, in: Fluvial Sedimentology VI, John Wiley & Sons, Ltd,](#)
168 [169–178, <https://doi.org/10.1002/9781444304213.ch13>, 1999.](#)

Formatted: Default Paragraph Font

169 Khalsa, S. J. S., Borsa, A., Nandigam, V., Phan, M., Lin, K., Crosby, C., Fricker, H., Baru, C., and Lopez, L.: OpenAltimetry
170 - rapid analysis and visualization of Spaceborne altimeter data, *Earth Sci Inform*, [https://doi.org/10.1007/s12145-020-00520-](https://doi.org/10.1007/s12145-020-00520-2)
171 [2](https://doi.org/10.1007/s12145-020-00520-2), 2020.

172 Kołaczek, P., Gałka, M., Apolinarska, K., Gębica, P., Superson, S., Michno, A., Harmata, K., Szczepanek, K., Płociennik, M.,
173 Gąsiorowski, M., Karpińska-Kołaczek, M.: Lost in dating – Problems with the absolute chronologies and sedimentation rates
174 of Late Glacial and Early Holocene oxbow lake deposits in Central Europe, *Quaternary Geochronology*, 41, 187-201,
175 <https://doi.org/10.1016/j.quageo.2017.05.002>.

176 Leeder, M. R.: A Quantitative Stratigraphic Model for Alluvium, with Special Reference to Channel Deposit Density and
177 Interconnectedness, 587–596, 1977.

178 Leier, A. L., DeCelles, P. G., and Pelletier, J. D.: Mountains, monsoons, and megafans, *Geology*, 33, 289–292,
179 <https://doi.org/10.1130/G21228.1>, 2005.

180 Lewis, G. W. and Lewin, J.: Alluvial Cutoffs in Wales and the Borderlands, in: *Modern and Ancient Fluvial Systems*, John
181 Wiley & Sons, Ltd, 145–154, <https://doi.org/10.1002/9781444303773.ch11>, 1983.

182 Mackey, S. D. and Bridge, J. S.: Three-dimensional model of alluvial stratigraphy; theory and applications, *Journal of*
183 *Sedimentary Research*, 65, 7–31, <https://doi.org/10.1306/D42681D5-2B26-11D7-8648000102C1865D>, 1995.

184 Makaske, B., Maathuis, B. H. P., Padovani, C. R., Stolker, C., Mosselman, E., and Jongman, R. H. G.: Upstream and
185 downstream controls of recent avulsions on the Taquari megafan, Pantanal, south-western Brazil, 37, 1313–1326,
186 <https://doi.org/10.1002/esp.3278>, 2012.

187 Martin, Harrison K.; Edmonds, Douglas A.: Martin and Edmonds Avulsion Model Supplemental Video 1, Supplemental videos
188 of the paper "The push and pull of abandoned channels: How floodplain processes and healing affect avulsion dynamics and
189 alluvial landscape evolution in foreland basins". <https://doi.org/10.5446/54887>

190 Martin, Harrison K.; Edmonds, Douglas A.: Martin and Edmonds Avulsion Model Supplemental Video 2, Supplemental videos
191 of the paper "The push and pull of abandoned channels: How floodplain processes and healing affect avulsion dynamics and
192 alluvial landscape evolution in foreland basins". <https://doi.org/10.5446/54888>

193 Martin, Harrison K.; Edmonds, Douglas A.: Martin and Edmonds Avulsion Model Supplemental Video 3, Supplemental videos
194 of the paper "The push and pull of abandoned channels: How floodplain processes and healing affect avulsion dynamics and
195 alluvial landscape evolution in foreland basins". <https://doi.org/10.5446/54889>

196 Martin, J., Sheets, B., Paola, C., and Hoyal, D.: Influence of steady base-level rise on channel mobility, shoreline migration,
197 and scaling properties of a cohesive experimental delta, 114, <https://doi.org/10.1029/2008JF001142>, 2009.

198 Mohrig, D., Heller, P. L., Paola, C., and Lyons, W. J.: Interpreting avulsion process from ancient alluvial sequences:
199 Guadalupe-Matarranya system (northern Spain) and Wasatch Formation (western Colorado), *GSA Bulletin*, 112, 1787–1803,
200 [https://doi.org/10.1130/0016-7606\(2000\)112<1787:IAPFAA>2.0.CO;2](https://doi.org/10.1130/0016-7606(2000)112<1787:IAPFAA>2.0.CO;2), 2000.

2201 [Moodie, A. J., Nittrouer, J. A., Ma, H., Carlson, B. N., Chadwick, A. J., Lamb, M. P., and Parker, G.: Modeling Deltaic Lobe-](#)
 2202 [Building Cycles and Channel Avulsions for the Yellow River Delta, China, 124, 2438–2462,](#)
 2203 <https://doi.org/10.1029/2019JF005220>, 2019.

2204 [Morón, S., Amos, K., Edmonds, D. A., Payenberg, T., Sun, X., and Thyer, M.: Avulsion triggering by El Niño–Southern](#)
 2205 [Oscillation and tectonic forcing: The case of the tropical Magdalena River, Colombia, GSA Bulletin, 129, 1300–1313,](#)
 2206 <https://doi.org/10.1130/B31580.1>, 2017.

2207 [Moudrý, V., Lecours, V., Gdulová, K., Gábor, L., Moudrá, L., Kropáček, J., and Wild, J.: On the use of global DEMs in](#)
 2208 [ecological modelling and the accuracy of new bare-earth DEMs, Ecological Modelling, 383, 3–9,](#)
 2209 <https://doi.org/10.1016/j.ecolmodel.2018.05.006>, 2018.

2210 [Nanson, G. C.: Point bar and floodplain formation of the meandering Beaton River, northeastern British Columbia, Canada,](#)
 2211 [27, 3–29, https://doi.org/10.1111/j.1365-3091.1980.tb01155.x](#), 1980.

2212 [Nanson, G. C. and Croke, J. C.: A genetic classification of floodplains, Geomorphology, 4, 459–486,](#)
 2213 [https://doi.org/10.1016/0169-555X\(92\)90039-Q](https://doi.org/10.1016/0169-555X(92)90039-Q), 1992.

2214 [Neuenschwander, A. L. and Pitts, K.: Ice, Cloud, and Land Elevation Satellite 2 \(ICESat-2\) Algorithm Theoretical Basis](#)
 2215 [Document \(ATBD\) for Land-Vegetation Along-Track Products \(ATL08\), https://nsidc.org/sites/nsidc.org/files/technical-](#)
 2216 [references/ICESat2_ATL08_ATBD_r003.pdf](#), 2020.

2217 [Neuenschwander, A. L., Pitts, K., Jelley, B. P., Robbins, J., Klotz, B., Popescu, S. C., Nelson, R. F., Harding, D., Pederson,](#)
 2218 [D., and Sheridan, R.: ATLAS/ICESat-2 L3A Land and Vegetation Height, version 3,](#)
 2219 <https://doi.org/10.5067/ATLAS/ATL08.003>, 2020.

2220 [O’Loughlin, F. E., Paiva, R. C. D., Durand, M., Alsdorf, D. E., and Bates, P. D.: A multi-sensor approach towards a global](#)
 2221 [vegetation corrected SRTM DEM product, Remote Sensing of Environment, 182, 49–59,](#)
 2222 <https://doi.org/10.1016/j.rse.2016.04.018>, 2016.

2223 [Paola, C., Heller, P. L., and Angevine, C. L.: The large-scale dynamics of grain-size variation in alluvial basins, 1: Theory, 4,](#)
 2224 [73–90, https://doi.org/10.1111/j.1365-2117.1992.tb00145.x](#), 1992.

2225 [Pelletier, J. D., Mayer, L., Pearthree, P. A., House, P. K., Demsey, K. A., Klawon, J. E., and Vincent, K. R.: An integrated](#)
 2226 [approach to flood hazard assessment on alluvial fans using numerical modeling, field mapping, and remote sensing, GSA](#)
 2227 [Bulletin, 117, 1167–1180, https://doi.org/10.1130/B25544.1](#), 2005.

2228 [Pizzuto, J. E.: Sediment diffusion during overbank flows, 34, 301–317, https://doi.org/10.1111/j.1365-3091.1987.tb00779.x,](#)
 2229 [1987.](#)

2230 [Pupim, F. do N., Assine, M. L., and Sawakuchi, A. O.: Late Quaternary Cuiabá megafan, Brazilian Pantanal: Channel patterns](#)
 2231 [and paleoenvironmental changes, Quaternary International, 438, 108–125, https://doi.org/10.1016/j.quaint.2017.01.013](#), 2017.

2232 [Ratliff, K. M., Hutton, E. H. W., and Murray, A. B.: Exploring Wave and Sea-Level Rise Effects on Delta Morphodynamics](#)
 2233 [With a Coupled River-Ocean Model, 123, 2887–2900, https://doi.org/10.1029/2018JF004757](#), 2018.

234 Ratliff, K. M., Hutton, E. W. H., and Murray, A. B.: Modeling long-term delta dynamics reveals persistent geometric river
 235 avulsion locations, *Earth and Planetary Science Letters*, 559, 116786, <https://doi.org/10.1016/j.epsl.2021.116786>, 2021.
 236 Reitz, M. D., Jerolmack, D. J., and Swenson, J. B.: Flooding and flow path selection on alluvial fans and deltas, 37,
 237 <https://doi.org/10.1029/2009GL041985>, 2010.
 238 Richards, K., Brasington, J., and Hughes, F.: Geomorphic dynamics of floodplains: ecological implications and a potential
 239 modelling strategy, 47, 559–579, <https://doi.org/10.1046/j.1365-2427.2002.00920.x>, 2002.
 240 Richardson, P. W., Perron, J. T., and Schurr, N. D.: Influences of climate and life on hillslope sediment transport, *Geology*,
 241 47, 423–426, <https://doi.org/10.1130/G45305.1>, 2019.
 242 Roering, J. J., Kirchner, J. W., and Dietrich, W. E.: Evidence for nonlinear, diffusive sediment transport on hillslopes and
 243 implications for landscape morphology, 35, 853–870, <https://doi.org/10.1029/1998WR900090>, 1999.
 244 Rossetti, D. F. and Valeriano, M. M.: Evolution of the lowest amazon basin modeled from the integration of geological and
 245 SRTM topographic data, *CATENA*, 70, 253–265, <https://doi.org/10.1016/j.catena.2006.08.009>, 2007.
 246 Rowland, J. C., Lepper, K., Dietrich, W. E., Wilson, C. J., and Sheldon, R.: Tie channel sedimentation rates, oxbow formation
 247 age and channel migration rate from optically stimulated luminescence (OSL) analysis of floodplain deposits, *Earth Surface*
 248 *Processes and Landforms*, 30, 1161–1179, <https://doi.org/10.1002/esp.1268>, 2005.
 249 Sadler, P. M.: Sediment Accumulation Rates and the Completeness of Stratigraphic Sections, *The Journal of Geology*, 89,
 250 <https://doi.org/10.1086/628623>, 1981.
 251 Schumde, T. H.: Some Aspects of Land Forms of the Lower Missouri River Floodplain, 53, 60–73, 1963.
 252 Schumer, R. and Jerolmack, D. J.: Real and apparent changes in sediment deposition rates through time, *Journal of Geophysical*
 253 *Research: Earth Surface*, 114, <https://doi.org/10.1029/2009JF001266>, 2009.
 254 Slingerland, R. and Kump, L.: *Mathematical Modeling of Earth's Dynamical Systems: A Primer*, Princeton University Press,
 255 246 pp., 2011.
 256 Slingerland, R. and Smith, N.: River avulsions and deposits, *Annual Review of Earth and Planetary Sciences*, 32, 257–285,
 257 <https://doi.org/10.1146/annurev.earth.32.101802.120201>, 2004.
 258 Smith, N., Slingerland, R., Pérez-Arlucea, M., and Morozova, G.: The 1870s avulsion of the Saskatchewan River, *Canadian*
 259 *Journal of Earth Sciences*, 35, 453–466, <https://doi.org/10.1139/cjes-35-4-453>, 1998.
 260 Steiger, J., Tabacchi, E., Dufour, S., Corenblit, D., and Peiry, J.-L.: Hydrogeomorphic processes affecting riparian habitat
 261 within alluvial channel–floodplain river systems: a review for the temperate zone, 21, 719–737,
 262 <https://doi.org/10.1002/rra.879>, 2005.
 263 Sun, T., Paola, C., Parker, G., and Meakin, P.: Fluvial fan deltas: Linking channel processes with large-scale morphodynamics,
 264 38, 26–1–26–10, <https://doi.org/10.1029/2001WR000284>, 2002.
 265 Toonen, W. H. J., Kleinhans, M. G., and Cohen, K. M.: Sedimentary architecture of abandoned channel fills, 37, 459–472,
 266 <https://doi.org/10.1002/esp.3189>, 2012.

Formatted: Default Paragraph Font

Formatted: Default Paragraph Font

Formatted: Default Paragraph Font

Formatted: Default Paragraph Font

1267 [Tooth, S., McCarthy, T. S., Brandt, D., Hancox, P. J., and Morris, R.: Geological controls on the formation of alluvial meanders](#)
 1268 [and floodplain wetlands: the example of the Klip River, eastern Free State, South Africa, 27, 797–815,](#)
 1269 <https://doi.org/10.1002/esp.353>, 2002.

1270 [Valenza, J. M., Edmonds, D. A., Hwang, T., and Roy, S.: Downstream changes in river avulsion style are related to channel](#)
 1271 [morphology, 11, 2116, https://doi.org/10.1038/s41467-020-15859-9, 2020.](#)

1272 [Weissmann, G., Hartley, A., Scuderi, L., Nichols, G., Davidson, S., Owen, A., Atchley, S., Bhattacharyya, P., Chakraborty,](#)
 1273 [T., Ghosh, A., Nordt, L., Michel, L., and Tabor, N.: Prograding distributive fluvial systems: Geomorphic models and ancient](#)
 1274 [examples, https://doi.org/10.2110/sepmsp.104.16, 1 January 2013.](#)

1275 [Weissmann, G. S., Hartley, A. J., Nichols, G. J., Scuderi, L. A., Olson, M., Buehler, H., and Banteah, R.: Fluvial form in](#)
 1276 [modern continental sedimentary basins: Distributive fluvial systems, Geology, 38, 39–42, https://doi.org/10.1130/G30242.1,](#)
 1277 [2010.](#)

1278 [Weissmann, G. S., Hartley, A. J., Scuderi, L. A., Nichols, G. J., Owen, A., Wright, S., Felicia, A. L., Holland, F., and Anaya,](#)
 1279 [F. M. L.: Fluvial geomorphic elements in modern sedimentary basins and their potential preservation in the rock record: A](#)
 1280 [review, Geomorphology, 250, 187–219, https://doi.org/10.1016/j.geomorph.2015.09.005, 2015.](#)

1281 [Wells, N. A. and Dorr, J. A.: A Reconnaissance of Sedimentation on the Kosi Alluvial Fan of India, 14, 1987.](#)

1282 [Wolman, M. G. and Eiler, J. P.: Reconnaissance study of erosion and deposition produced by the flood of August 1955 in](#)
 1283 [Connecticut, 39, 1–14, https://doi.org/10.1029/TR039i001p00001, 1958.](#)

1284 [Wolman, M. G. and Leopold, L. B.: River flood plains: Some observations on their formation, River flood plains: Some](#)
 1285 [observations on their formation, U.S. Government Printing Office, Washington, D.C., https://doi.org/10.3133/pp282C, 1957.](#)

1286 [Wren, D. G., Davidson, G. R., Walker, W. G., and Galicki, S. J.: The evolution of an oxbow lake in the Mississippi alluvial](#)
 1287 [floodplain, Journal of Soil and Water Conservation, 63, 129-135, https://doi.org/10.2489/jswc.63.3.129, 2008.](#)

1288 [Zani, H., Assine, M. L., and McGlue, M. M.: Remote sensing analysis of depositional landforms in alluvial settings: Method](#)
 1289 [development and application to the Taquari megafan, Pantanal \(Brazil\), Geomorphology, 161–162, 82–92,](#)
 1290 <https://doi.org/10.1016/j.geomorph.2012.04.003>, 2012.

1291 [Zwoliński, Z.: Sedimentology and geomorphology of overbank flows on meandering river floodplains, Geomorphology, 4,](#)
 1292 [367–379, https://doi.org/10.1016/0169-555X\(92\)90032-J, 1992.](#)

Formatted: Default Paragraph Font